



Damage zones induced by in situ stress unloading during excavation of diversion tunnels for the Jinping II hydropower project

Y. Fan¹ · J. W. Zheng¹ · X. Z. Cui¹ · Z. D. Leng^{1,2} · F. Wang¹ · C. C. Lv¹

Received: 30 October 2020 / Accepted: 1 March 2021 / Published online: 19 March 2021
© Springer-Verlag GmbH Germany, part of Springer Nature 2021

Abstract

During the excavation of deep tunnels with high in situ stress, the stress unloading path caused by the rock mass excavation has important influences on the formation of the EDZ (excavation damage zone). In this study, the project background of the Jinping II diversion tunnels was firstly introduced. Then, the influences of stress unloading path induced by blasting excavation and tunnel boring machine (TBM) excavation on the EDZ were analyzed based on the acoustic data. Finally, the effects for different unloading paths of in situ stress induced by different excavation methods on the EDZ were studied by theoretical calculation and numerical simulation. The results show that compared with the quasi-static unloading, the transient unloading amplifies the effects of radial stress unloading and the tangential stress loading in surrounding rock masses. The EDZ depths of the blasting excavation tunnel are about 1.0 m greater than those of the TBM excavation tunnel. Moreover, the depths of the low-velocity band of the blasting excavation tunnel account for more than 50% of the total EDZ depths, while the depths of the low-velocity band of the TBM excavation tunnel account for about 30% of the total EDZ depths. The distribution of the low-velocity band along the excavation contour is closely related to the secondary stress field, indicating that the transient unloading of in situ stress is one of the important causes of the low-velocity band. After considering the post-peak mechanical properties of marble, the EDZ extents induced by different excavation methods can be estimated through numerical simulation.

Keywords Deep tunnel · Excavation damage zone (EDZ) · Quasi-static unloading · Transient unloading · High in situ stress

Introduction

In order to meet the huge energy needs of the growing population and booming economy, China has constructed a number of large and oversize hydropower projects in the western region of the country. However, due to the terrain conditions of the alpine canyons in southwestern China, these projects all require the high-intensity, large-scale rock excavation for ultra-long tunnels or large-span cavern groups in harsh geological environments. During the excavation process, the

excavated rock mass spalls from the original rock surface, causing the abrupt removal of the stress constraint on the retained rock mass, and the initial stress state of the rock mass near the excavation surface is broken and leads to the stress redistribution, which causes new cracks in the rock mass and the opening of the original cracks in the rock mass (Martino and Chandler 2004; Siren et al. 2015). Especially when the depth of excavation area is relatively high, the in situ stress will also be inevitably high, and this will induce more drastic stress adjustment process and more damage in the retained rock mass after excavation (Hao et al. 2016; Liu et al. 2020). Then, coupled with external factors, such as the excavation load and groundwater, the existing environment and the mechanical characteristics of the surrounding rock mass deteriorate and the excavation damage zone (EDZ) is formed in the surrounding rock mass. In the EDZ, the physical properties, mechanical properties, and permeability characteristics of the rock mass are degraded, which leads to the geological disasters such as the collapse, fault fracture zone, support failure, seepage, large deformation, and rockburst (Kwon et al. 2009; Zhang et al. 2015; Xu et al. 2018; Bao et al. 2019; Sun et al.

✉ J. W. Zheng
jjunweizheng@163.com

✉ Z. D. Leng
zdleng@whu.edu.cn

¹ Hubei Key Laboratory of Construction and Management in Hydropower Engineering, China Three Gorges University, Yichang 443002, China

² China Gezhouba Group Explosive Co. Ltd, Chongqing 401121, China

2020). Hence, studying the characteristics and evolution of the EDZ has practical significance and theoretical value to optimizing the supporting parameters, ensuring safe construction, and evaluating the engineering stability of deep tunneling.

Many previous studies have been conducted on the EDZ of the surrounding rock mass and achieved fruitful results. Several studies ran numerical simulations and conducted field tests of the excavation damage zone and found that the changes in the magnitude and direction of the stress field of the surrounding rock mass (stress redistribution of the surrounding rock mass) caused by the excavation are an important cause of the excavation damage (Read et al. 1995; Martin 1997; Blümling et al. 2007; Kwon et al. 2009; Yong et al. 2013; Vazaios et al. 2019). As early as 1966, Cook et al. (1966) determined that for the excavation response of the surrounding rock mass to the unloading of the deep rock mass, due to the transient release of the original stress of the rock mass during excavation, the phenomenon of over relaxation will occur and produce tensile stress in the rock mass. Diederichs (2007) indicated that during hard rock excavation in large burial depths and high in situ stress, the excavation response is complicated by brittle fracture. However, under the low constraint of the excavation boundary, the high-intensity compressive stress generates tensile cracks, and the main failure mechanism is controlled by the tensile strength of the rock mass. With the development of numerical simulation technology, a massive number of new numerical simulation methods and damage constitutive models have been

developed, which provide a powerful means of studying deep rock EDZ. For instance, Pellet et al. (2009) and Mortazavi and Molladavoodi (2012) employed a damage model to simulate the formation and evolution of the EDZ. Wang et al. (2019) adopted a binary linear regression model to determine the relationships between the change in the range of the EDZ and the excavation span, rock characteristics, and burial depth. Souley et al. (2018) employed a non-linear constitutive model, which takes into account the more realistic mechanical behavior of hard rock to predict the expansion of the EDZ around the tunnel.

It should be noted that most of the described studies above generally regarded excavation unloading as a quasi-static process in the analysis of the excavation response and mechanical effects of the rock mass. However, these analysis methods are more applicable to rock mass under lower stress levels. Many recent studies have shown that for deep rock mass with a high in situ stress level, the duration of the excavation unloading is only a few milliseconds, which indicates a typical transient unloading process. Thus, the dynamic effects of transient unloading on the rock mass along the excavation contour should not be ignored (Lu et al. 2012; Li et al. 2014). Zhu et al. (2014) indicated that the stress redistribution of the surrounding rock mass caused by blasting excavation of deep tunnels is a dynamic process, and it has significant impacts on the distribution of the EDZ. Yang et al. (2017, 2018) demonstrated that during blasting excavation, the rapid release of the stress on the excavation boundary generates additional stress fluctuations, resulting in greater deviatoric stress,

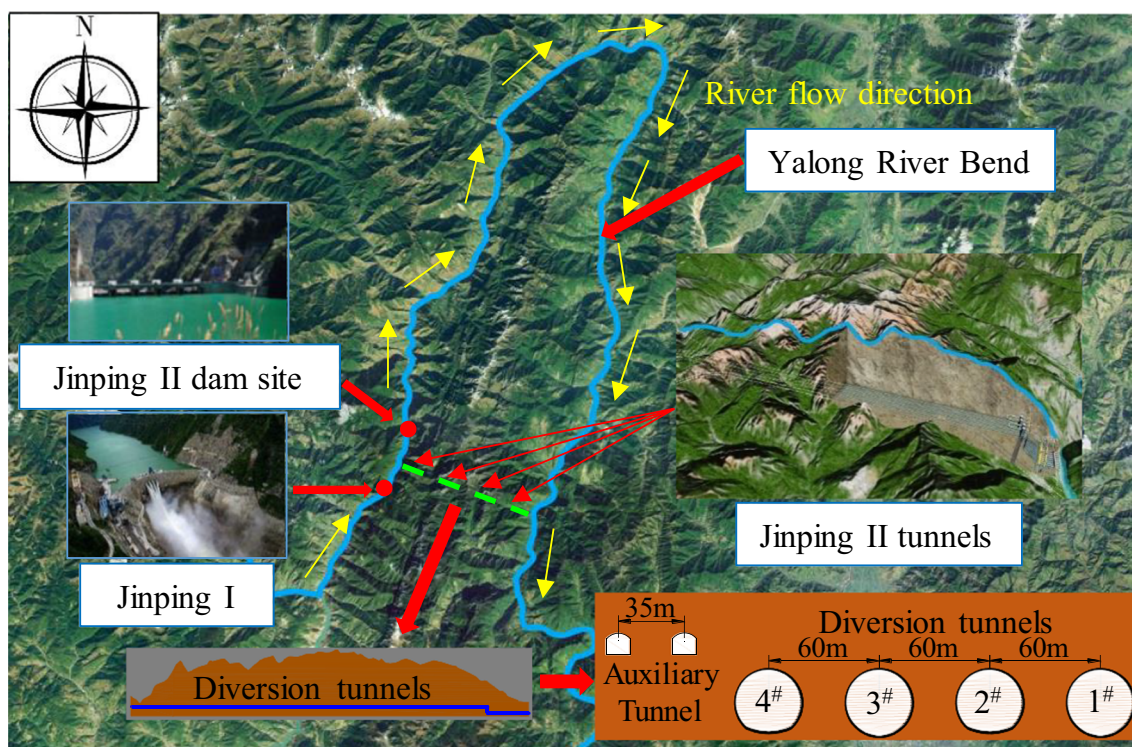


Fig. 1 Location and tunnel distribution of the Jinping II hydropower project

which leads to the surrounding rock mass more likely damaged. Thus, the treatment regarding the unloading of in situ stress as a quasi-static process leads to large errors.

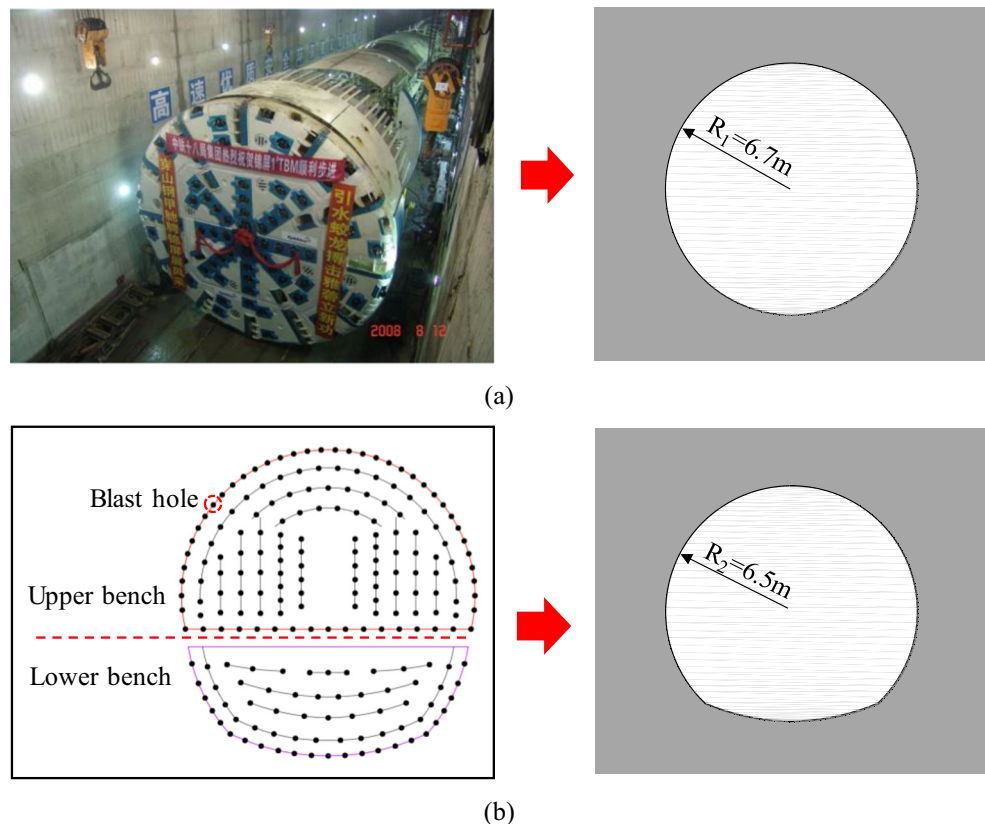
The purpose of this paper is to analyze the formation mechanism and distribution of EDZ induced by the excavation of the diversion tunnels of the Jinping II hydropower project. First, the in situ stress field distribution and geological conditions along the diversion tunnels of the Jinping II hydropower project were investigated. Then, the stress unloading mechanisms of the surrounding rock mass for the cases of the tunnel boring machine (TBM) excavation method and the blasting excavation method were analyzed in combination with previous studies. On the basis of the above, we adopted theoretical analysis to calculate the dynamic stress field induced by the quasi-static unloading of in situ stress and the transient unloading of in situ stress under a hydrostatic stress field. Then, the Fast Lagrangian Analysis of Continua 3D (FLAC3D) was employed to simulate the evolution law of the EDZ under a non-hydrostatic stress field, and the correctness of the numerical simulation method was verified by the damage detection results of the Canadian underground research laboratory (URL). Finally, based on the results of the field tests for the diversion tunnels of the Jinping II hydropower project and the results of the numerical simulation, the effects of the TBM excavation method and the blasting excavation method on the distribution of the EDZ were analyzed.

Project background

The Jinping II hydropower project is located at the river bend on the mainstream of the Yalong River, Sichuan Province, China (Fig. 1). There are several deeply buried and parallel tunnels through the Jinping Mountains, which cut the river bend and utilize the highly natural drop for power generation. The deeply buried tunnel group is composed of four diversion tunnels with an average length of 16.67 km, two auxiliary tunnels with an average length of 17.5 km, and one water drainage tunnel. Construction started on the main project in January 2007, and the first generator started operating in August 2013. By the end of 2014, all of the generators were put into operation for power generation, and the total installed capacity of the power station was 4800 MW.

To reduce the excavating disturbance between the adjacent tunnels during tunnel excavation, two diversion tunnels were excavated by tunnel boring machine (TBM), and the other two were excavated by blasting. For instance, diversion tunnels 1[#] and 3[#] were excavated using TBM, which is the 410–319 open TBM produced by Robbins Company of the USA and is designed with straight cutter head. The support system of TBM is divided into three zones: zone L1 is the emergency safety support zone, which can be supported with an anchor rod,

Fig. 2 Schematic diagrams of the TBM excavation and blasting excavation of the diversion tunnels. **a** TBM excavation diagram (Wu et al. 2015). **b** Blast hole layout of the blasting excavation.



steel mesh, steel arch frame, steel tile, and shotcrete; zone L2 is the main support zone, which can be supported with an anchor and shotcrete; zone L3 is a reinforced support area, which can be supported with shotcrete (Fig. 2a) (Wu et al. 2015). The excavation section was circular with a diameter of 13.4 m. Diversion tunnels 2[#] and 4[#] were excavated adopting the blasting method, and the excavation section is horseshoe-shaped with a diameter of 13.0 m. During the blasting excavation, first, the upper bench of the tunnel section was excavated with a height of 7.5 m, and then, the lower bench was excavated with a height of 5.5 m. The layout of blast holes for diversion tunnel 2[#] is shown in Fig. 2b.

The diversion tunnel group passes through the geologically complex Jinping Mountain, and the lithology along the tunnel mainly includes Middle and Upper Triassic marble, limestone, sandstone, and slate. From east to west, the tunnels pass through the strata of the Yantang Group (T_{2y}), Baishan Group (T_{2b}), Upper Triassic (T₃), Zagunao Group (T_{2z}), and Lower Triassic (T₁) (Fig. 3a). Based on the lithological difference in the same strata, several complex strata were subdivided. For instance, the Yantang Group (T_{2y}) is divided into the T_{2y}¹–T_{2y}⁶ 6 layers, and the Upper Triassic (T₃) is divided into the T₃¹–T₃³ 3 layers. In addition, the distribution directions of the in situ stress in the project area are shown in Fig. 4. As can be seen from Fig. 4, the maximum horizontal in situ stress (structural stress) is mainly oriented NW–NWW, and the structural trace and distribution direction under the control of the stress field can be divided into four structural groups: NNE orientation, NNW orientation, NE–NEE orientation, and NW–NWW orientation. The distributions of the lithology, faults, surrounding rock classifications, and fold structures are shown in Fig. 3b.

The main elevation of Jinping Mountain is more than 4000 m, the summit has an elevation of 4488 m, and the maximum height difference is more than 3000 m. Consequently, most of the areas of the diversion tunnels are in the high burial depth, and the maximum burial depth is 2525 m. The high burial depth inevitably results in the rock mass being under high in situ stress levels. To measure the in situ stress along the Jinping II diversion tunnel, a number of measuring points were arranged at the western and eastern part of Jinping auxiliary tunnel at the early stage of tunnel excavation, and the in situ stress of measuring points is measured by a hydraulic fracturing method. According the measured data, the whole in situ stress field along the Jinping II diversion tunnel was calculated (see Fig. 5). In Fig. 5, the maximum principal stress (σ_{\max}) is as high as 72 MPa, and the stress direction is parallel to the tunnel axis. The minimum principal stress (σ_{\min}) is as high as 32 MPa in the vertical direction. The middle principal stress (σ_{mid}) is as high as 34 MPa and is perpendicular to the tunnel axis.

Fig. 3 Geological structures along the diversion tunnel of the Jinping II hydropower project. **a** Plan view of the geological structures along the tunnel. **b** Profile view of the geological structures along the tunnel

EDZ of the diversion tunnels at the Jinping II hydropower project

Acoustic detection scheme

Engineering detection methods for EDZ include rock mass mechanical parameter (seismic wave velocity, acoustic velocity, elastic modulus, and permeability rate) contrast detection before and after excavation and borehole television. Among them, the acoustic velocity detection method has been widely used in the engineering industry due to its high accuracy. This method usually adopts the variation rate of the longitudinal wave velocity η of the rock mass as the criterion for the extent of the excavation damage:

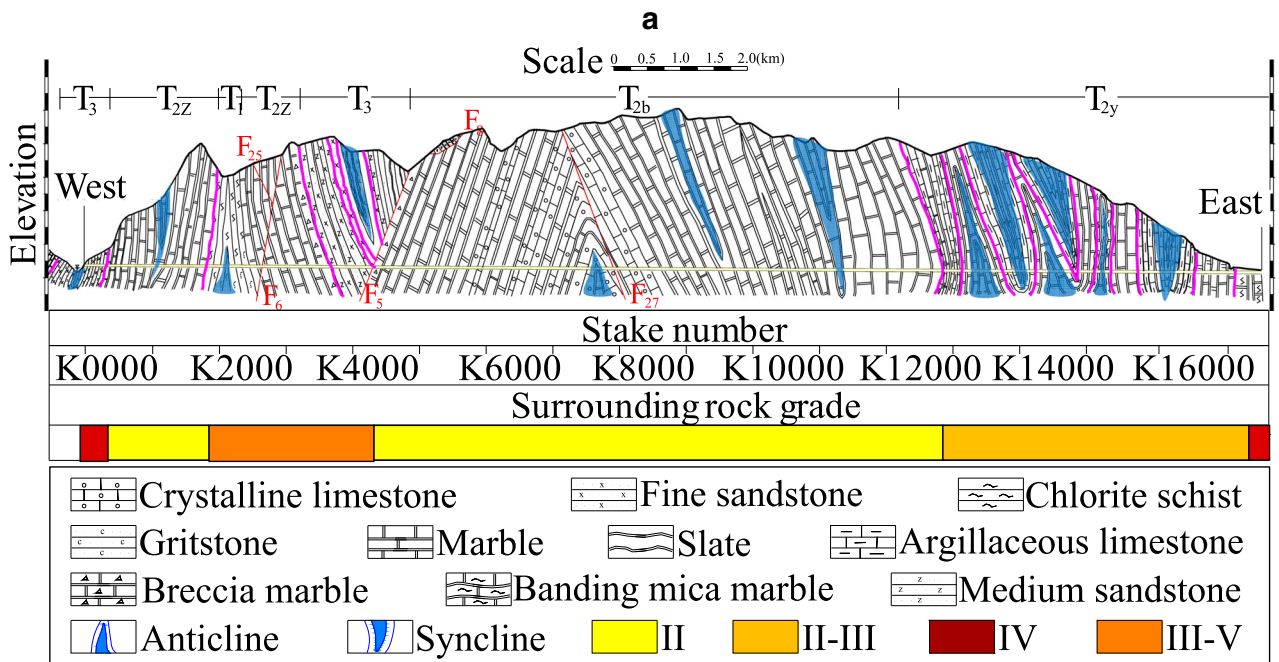
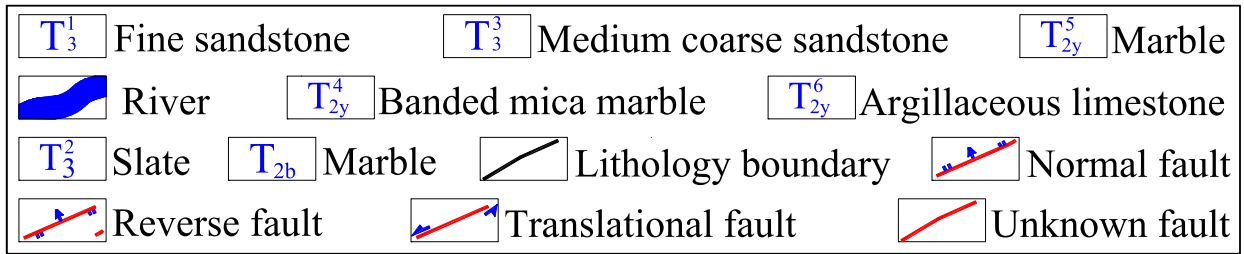
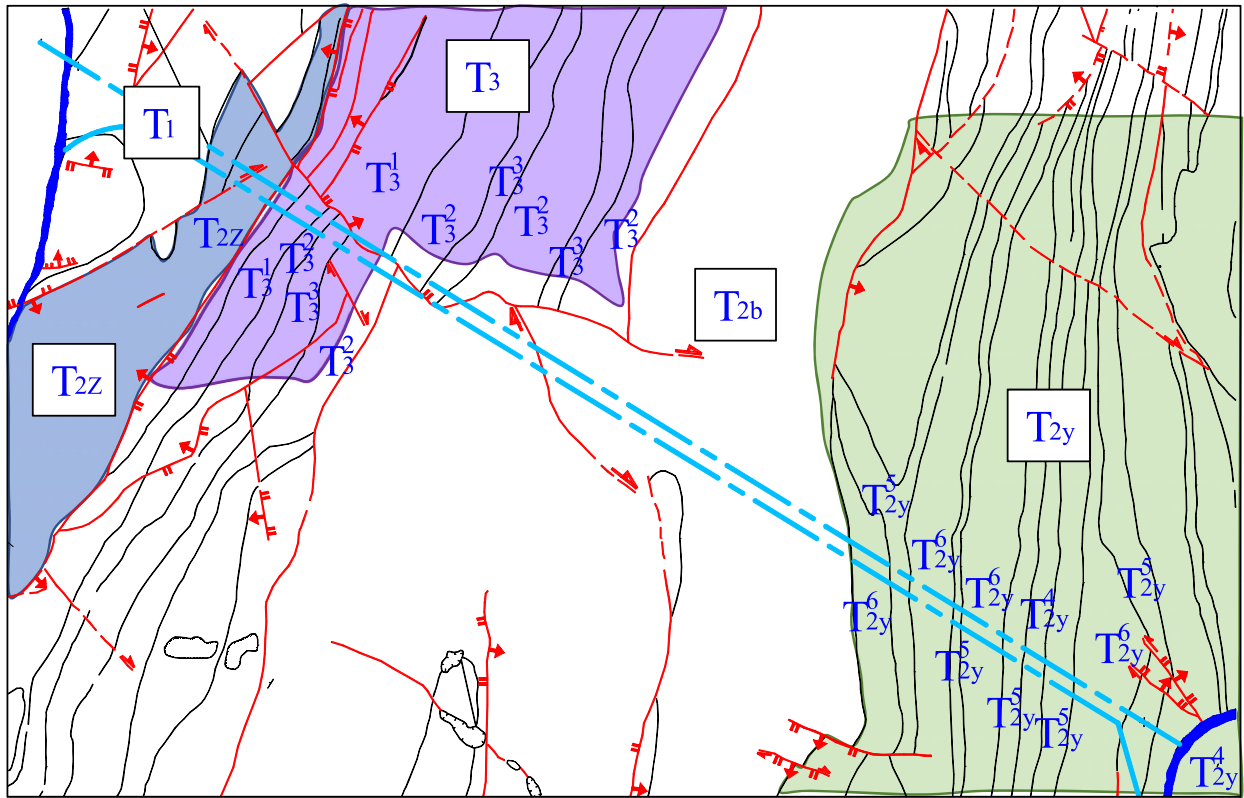
$$\eta = (C_0 - C_1) / C_0 \quad (1)$$

where C_0 is the average longitudinal wave velocity of the surrounding rock mass in the undisturbed area, and C_1 is the longitudinal wave velocity of the surrounding rock mass at the current depth.

According to the *Construction Specification on Underground Excavating Engineering of Hydraulic Structures (DL/T 5099-1999)*, when the longitudinal wave velocity of the rock mass is decreased by more than 10% of the average longitudinal wave of the undisturbed rock mass, the rock mass can be regarded as being damaged. The greater the velocity reduction, the more intense the damage.

In this paper, the single-hole acoustic velocity detecting method was adopted to detect the EDZ of the diversion tunnels of the Jinping II hydropower project, and the detecting instrument used was the RS-ST01C sonic instrument produced by Rock Sea Company, Wuhan, China. The directions of the detecting holes were arranged perpendicular to the direction of the free face, and continuous detections were carried out along the tunnel wall from bottom to top with an interval of 0.2 m. The detecting instrument and field tests are shown in Fig. 6.

According to the shape of the tunnel section, the axis direction of the tunnel, the geological conditions, and the excavation method, several sections of diversion tunnel 1[#] (TBM excavation) and diversion tunnel 2[#] (blasting excavation) were selected for research. The detection schemes are shown in Fig. 7. As can be seen from Fig. 7, five detection holes (10 m in depth and 76 mm in diameter) were arranged around the tunnel section. The detection holes were numbered clockwise from left to right (the left side is the left-hand side in the direction of the river flow (north side), and the right side is



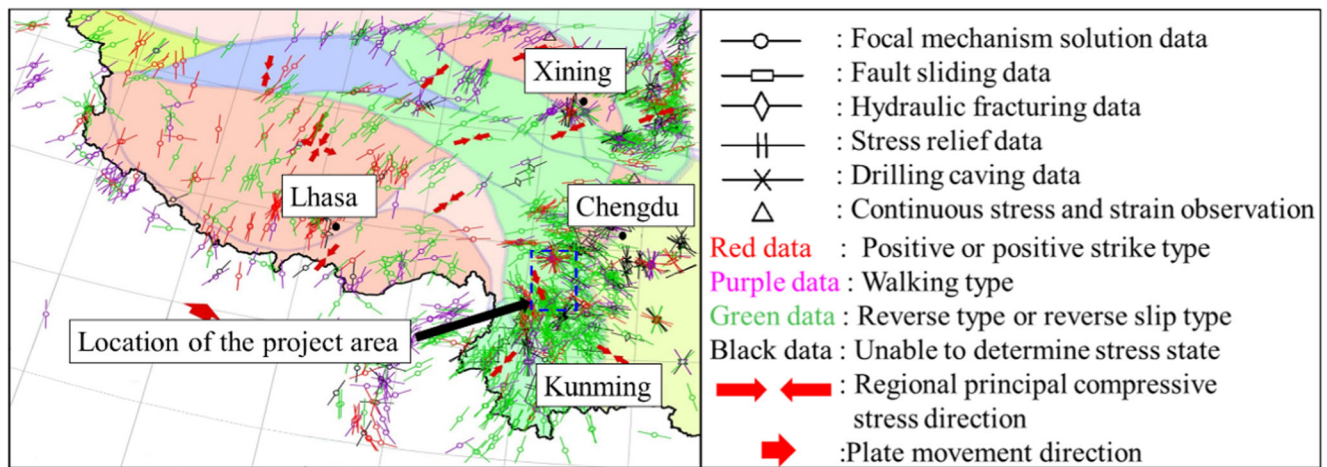


Fig. 4 In situ stress at the location of the Jinping II hydropower project

the right-hand side in the direction of the river flow (south side)).

Acoustic detection results

The locations of the detection sections in diversion tunnel 1[#] are given in Fig. 8, and the acoustic data for the detection holes in these sections are shown in Fig. 9. The damage zone extents of each detection hole were obtained based on the acoustic data (Table 1).

As can be seen from Table 1 and Fig. 9, the extents of the EDZ for the detection sections in diversion tunnel 1[#] vary from 1.2 to 3.0 m, and the EDZ distribution of the tunnel sections is uniform. The EDZ surrounding the detecting section has a wider distribution on the northern arch (the upper left side) of the tunnel section, which illustrates the influence of the secondary stress field on the distribution of the EDZ.

To compare with the detection sections in diversion tunnel 1[#], five sections in diversion tunnel 2[#] (Fig. 10) were selected for acoustic detection. The detection results are shown in Table 2 and Fig. 11.

As can be seen from Table 2 and Fig. 11, for the tunnel section excavated by blasting, the largest damage extent of section K15700 is in the southern arch, while the largest damage extent of section K15505 is in the northern arch, so the damage extent is not completely influenced by the secondary

stress field. This demonstrates that the excavation response caused by the blasting excavation also plays an important role in the formation of the EDZ. During acoustic detection, the lower bench of sections K14500, K14245, and K13880 was not excavated, and thus, only three detection holes in the upper bench were tested. However, the maximum damage extents of these three sections are not distributed in the northern arch, which indicates that the formation of the EDZ in the blasting excavation section is not only related to the secondary stress field, but it is also closely related to the shape of the excavation section, the excavation method, and other factors. Besides, by comparing the test results for each of the sections in diversion tunnel 1[#] and diversion tunnel 2[#] (Tables 1 and 2), we found that for section K15700 (in diversion tunnel 1[#]) and section K15700 (in diversion tunnel 2[#]), for similar lithologies, geological structures, and burial depths, the damage extents caused by TBM excavation vary from 1.8 to 3.0 m, while the damage extents caused by blasting excavation vary from 2.8 to 4.2 m. Similarly, the damage extents caused by the TBM excavation of section K14280 are 1.2–1.8 m, and the damage extents caused by the blasting excavation of section K14500 are 2.2–2.8 m. Thus, under similar conditions, the damage extents caused by blasting excavation are larger than those caused by TBM excavation, which further indicates that blasting excavation aggravates the damage to the surrounding rock mass.

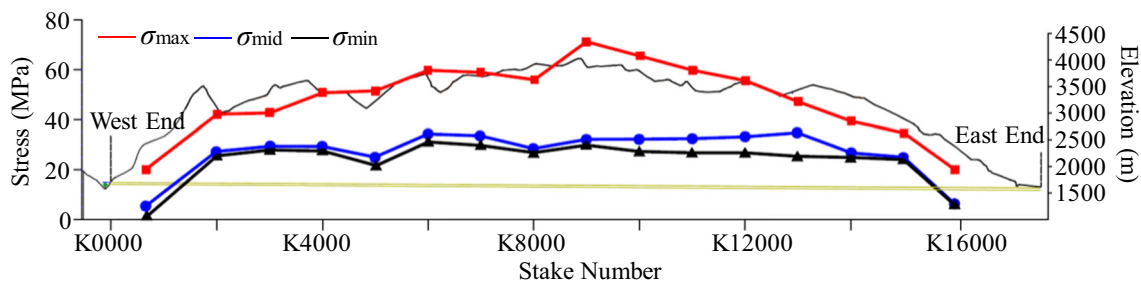


Fig. 5 In situ stress field along the diversion tunnel of the Jinping II hydropower project

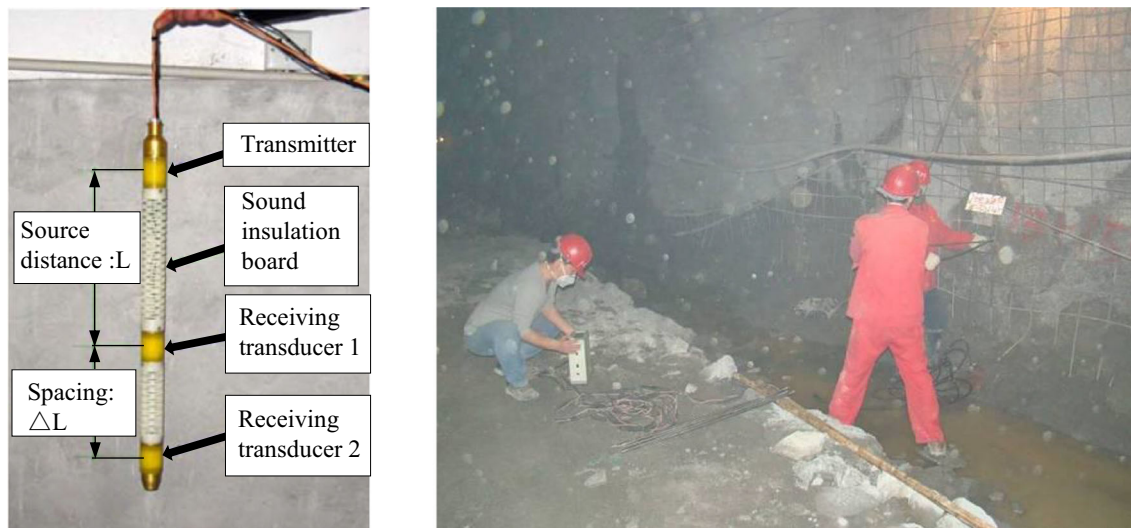


Fig. 6 Acoustic detecting instruments and field tests of the diversion tunnels of the Jinping II hydropower project

As can be seen from Table 2, for the same excavation method, burial depth, and in situ stress level, the extents of the EDZ detected in the excavation sections of the class II surrounding rock mass (K15505 1.6–2.8 m, K14245 1.8–2.2 m) are less than those detected in the excavation sections of the class III surrounding rock mass (K15700 2.8–4.2 m, K14500 2.2–2.8 m). Therefore, compared with the class II surrounding rock mass, the class III surrounding rock mass with poor quality is more likely to be damaged after excavation, which indicates that the quality of the rock mass is also an important factor affecting the distribution of the EDZ. Based on Figs. 9 and 11 and the comparison of the acoustic detection results of the excavation damage zones of section K15700 with section K15505 and section K14500 with section K14245 in the diversion tunnel 2[#], it can be found that for the excavation section in the same fold wing, the extents of the EDZ detected in the excavation section of the class II surrounding rock mass are smaller. This illustrates that the extents of the excavation damage zones in the class II surrounding rock mass with better rock mass quality are less affected by the fold structure, and the influence of the fold structure on

the class III surrounding rock mass with a worse rock mass quality is more obvious. Finally, according to the acoustic detection results for diversion tunnel 1[#] and diversion tunnel 2[#], for both excavation methods, as the buried depth and in situ stress level increase, the extents of the EDZ of each section gradually decrease; it indicates that the influence of the fold structure on the extents of EDZ gradually weakens with the increase of confining pressure.

Influence of different unloading paths of in situ stress induced by excavation method on formation of EDZ

Based on the preliminary analysis of the acoustic data for each detection section of diversion tunnel 1[#] and diversion tunnel 2[#] and the comparison of the data in Figs. 9 and 11, it can be further found that during TBM excavation, the acoustic velocities of the rock mass in the damage zone transit smoothly from the excavation surface into the surrounding rock mass, whereas the transition is obviously slow during blasting excavation. And there is a significant low-velocity zone near the excavation surface, which indicates that the blasting

Fig. 7 Arrangement of the acoustic detection holes in the diversion tunnels

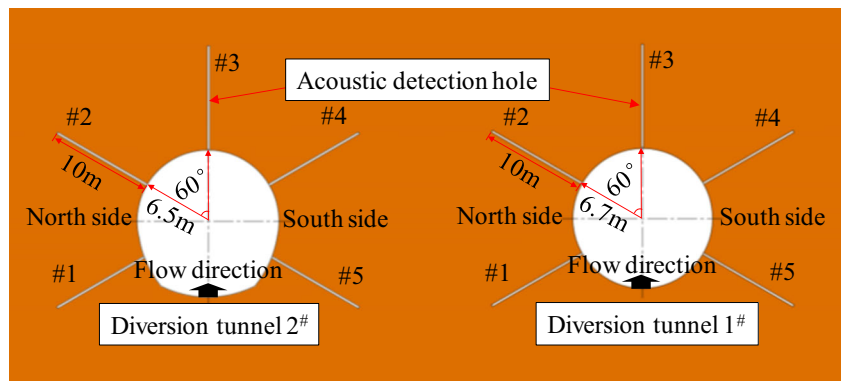
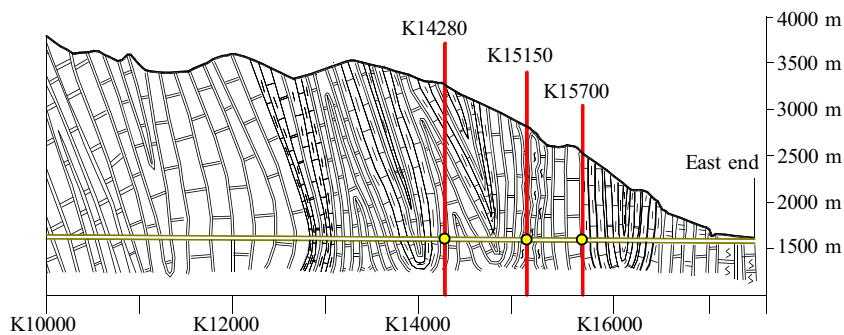


Fig. 8 Positions of the detection sections of diversion tunnel 1[#]



excavation induces severer damage around the excavation contour. It is widely acknowledged that due to deep-buried

depth of the surrounding rock mass for the Jinping diversion tunnel, the surrounding rock mass is highly stressed, and it

Fig. 9 Detection results for the detecting sections in diversion tunnel 1[#]. **a** Section K15700. **b** Section K15150. **c** Section K14280

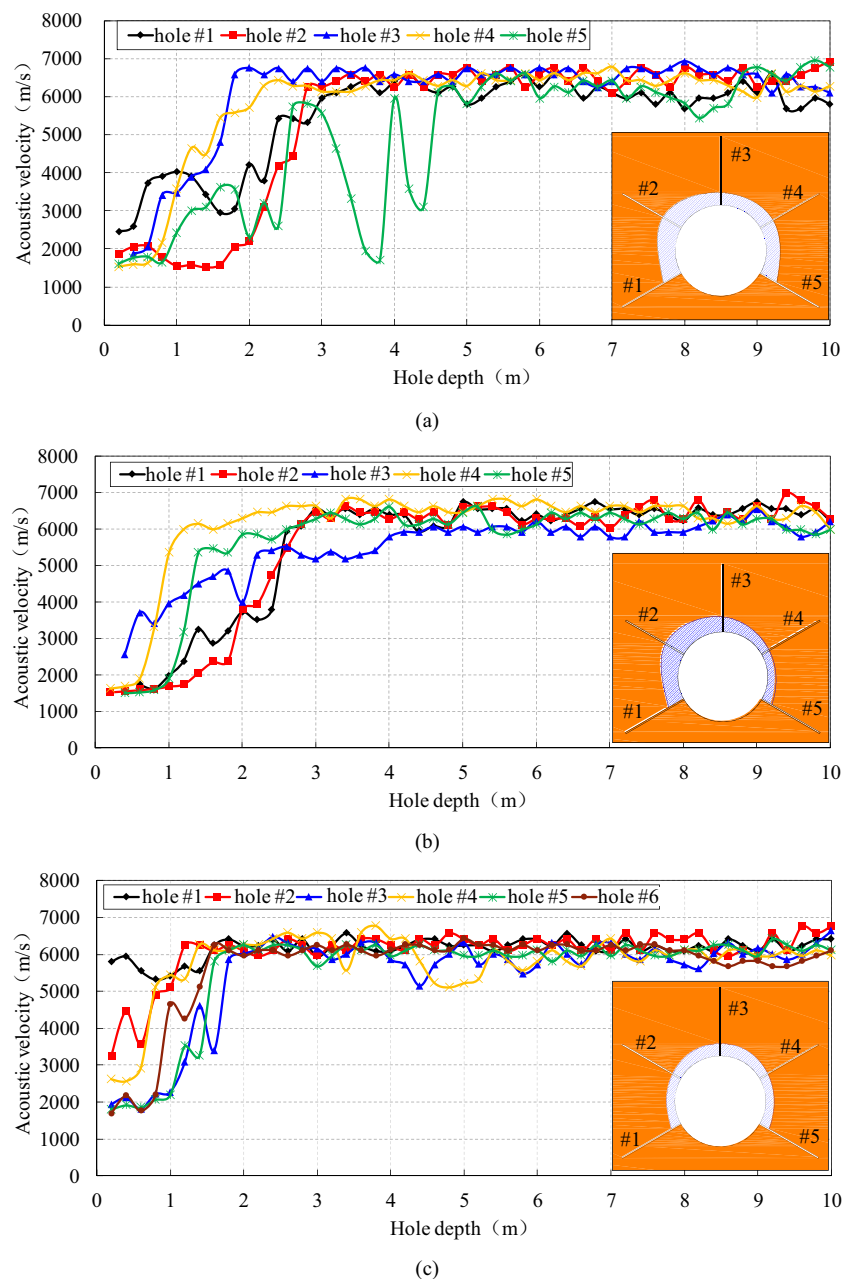


Table 1 Detection results for the detection section in diversion tunnel 1[#]

Positions of the detection sections	Lithology	Surrounding rock classification	Burial depth (m)	Hole #1	Hole #2	Hole #3	Hole #4	Hole #5	
Extents of damage zone (m)	K15700	T _{2y} ⁵	II	1092	3.0	2.8	1.8	2.2	2.8
	K15150	T _{2y} ⁴	III	1400	2.6	2.8	2.2	1.2	1.4
	K14280	T _{2y} ⁵	III	1750	1.6	1.2	1.8	1.4	1.6

will induce a dramatic stress adjustment in the surrounding rock mass after excavation. The different excavation method such as TBM excavation and blasting excavation will cause different unloading paths of in situ stress on the excavation boundary, which causes different influences on the rock damage (Tao et al. 2013). In the following sections, the characteristics of acoustic data and the influence of stress unloading path caused by TBM excavation and blasting excavation on EDZ will be investigated.

Composition of EDZ

According to the acoustic detection data and the determination of the surrounding rock damage zone obtained in “Acoustic detection results,” the acoustic velocity of the damage zone can be divided into bands: the low-velocity band and the transition velocity band. The methods and results of defining the low-velocity band and the transition velocity band for the TBM-excavated sections are shown in Fig. 12 and Table 3, respectively.

As can be seen from Table 3 and Fig. 12, for the tunnel sections excavated by TBM, the acoustic velocities of the rock mass in the damage zone gradually and smoothly transit from the excavation surface into the surrounding rock mass. Compared with the depths of the transition velocity band, the depths of the low-velocity band are significantly shallower, and the absolute depths are primarily within 0.80 m, which only accounts for 23–57% of the total depths of the damage zone, with the majority accounting about 25%. Based on the distribution characteristics of the low-velocity bands along the excavation contour, the low-velocity bands are affected by the secondary stress field, which is larger on the upper left arch (the northern arch). The transition velocity bands are the main part of the damage zones in diversion tunnel 1[#], and the acoustic velocity of the rock mass gradually transits to the acoustic velocity of the undisturbed rock mass. According to the research results of the URL, this part of the damage zone is mainly caused by the stress redistribution, which leads to the transition velocity bands becoming the main object of interest in the reinforcement of the surrounding rock mass and the support treatment of the tunnel.

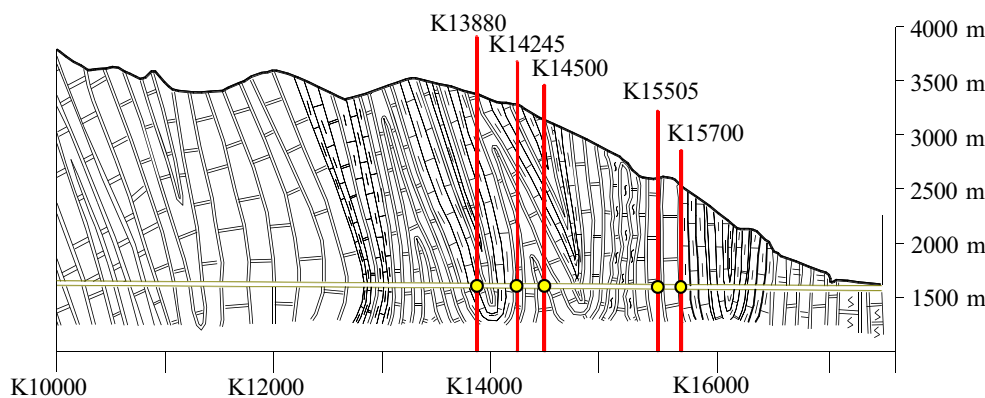
The methods and results of delimiting the low-velocity bands and transition velocity bands in the blasting excavated sections are shown in Fig. 13 and Table 4.

As can be seen from Fig. 13 and Table 4, the depths of the low-velocity bands in the EDZ of diversion tunnel 2[#] are primarily greater than 1.0 m, and most account for more than 50% of the total depths of the damage zone. This differs significantly from the results for the TBM-excavated sections. It can also be found from Fig. 13 that the distribution of low-velocity bands of diversion tunnel 2[#] around the tunnel section is strongly affected by the secondary stress field. According to the research conclusion of URL in Canada, if the formation of the low-velocity bands (severe damage zone) is only caused by the blasting load, then the low-velocity bands should evenly distribute around the tunnel section (Martin et al. 1997; Read 2004). Therefore, the formation of low-velocity bands during blasting excavation of tunnels with high in situ stress condition should also be related the stress adjustment induced by unloading of in situ stress.

According to the distribution of the in situ stress along the diversion tunnels (Fig. 5), as the burial depth and in situ stress level increase, the ratios of the low-velocity band depths to the total damage depths for diversion tunnel 1[#] increase from 27–29% to 31–67%. The ratios of low-velocity band depths to the total damage depths of diversion tunnel 2[#] increase from 29–50% to 50–68%. It can be found that for the diversion tunnel 1[#], the minimum ratio of low-velocity bands increases by only 4%, while the maximum ratio of low-velocity bands increases significantly by 38%. For the diversion tunnel 2[#], both the minimum and maximum proportions of the low-velocity band increase by about 20%. These further indicate that the stress unloading under high in situ stress is the direct cause of low wave velocity zone, and the unloading of high in situ stress induced by blasting excavation will intensify the generation of low-velocity bands. Thus, it can be further concluded that due to high in situ stress, large magnitude and fast unloading of in situ stress will induce larger low-velocity damage zones, which proves that the damage zones measured in the TBM-excavated tunnel and blasting excavated tunnel are mainly caused by the unloading of the in situ stress (Falls and Young 1998; Young et al. 2000; Zhu et al. 2014; Yang et al. 2018).

According to Table 4, compared with the class III surrounding rock mass (K15700 29~57% and K14500 36~42%), the ratios of the depths of the low-velocity bands of the EDZ of the class II surrounding rock mass (K15505 50~72% and K14245 55~67%) to the total depths of damage

Fig. 10 Positions of the detection sections of diversion tunnel 2[#]



zone are larger. This indicates that during blasting excavation, the class II surrounding rock mass which has a better rock mass quality is more likely to form low-velocity bands after excavation.

Although the detection results of EDZ at the test section prove the contribution of the stress adjustment effect induced by the blasting excavation to the EDZ in the surrounding rock mass from another perspective, it is not intuitive because the effect of blasting load cannot be eliminated. In the following sections, theoretical calculation and numerical calculation are supplemented to compare the influences of stress unloading paths induced by blasting excavation and TBM excavation on the EDZ.

In situ stress unloading caused by blasting excavation and TBM excavation

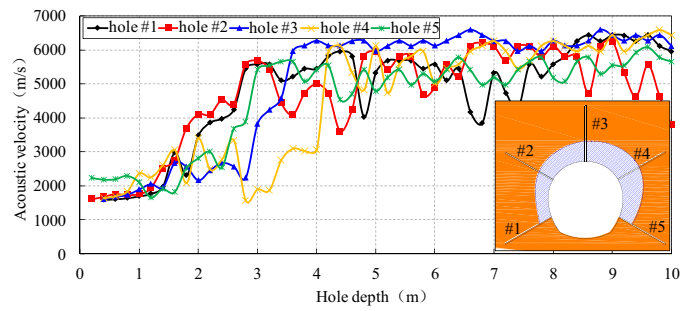
It is generally accepted that there is significant difference between the unloading forms of high in situ stress induced by blasting excavation and TBM excavation. As the strain rate is usually taken as the criterion to determine whether a loading process is a quasi-static one, the unloading time of in situ stress caused by blasting excavation and TBM excavation should be calculated at first. According to Lu et al.’s study and the excavation parameters (tunneling rate) of the TBM excavation of the Jinping construction drainage tunnel (Table 5), the unloading time of in situ stress and strain rate caused by blasting excavation and

TBM excavation with high in situ stress was calculated, as shown in Table 6 (Lu et al. 2012). As can be seen from Table 6, the strain rate caused by blasting excavation is significantly higher than that induced by TBM excavation under the condition of high in situ stress. When the strain rate is greater than $10^{-1}/s$, then the effect of the inertial force cannot be ignored, and the unloading of the in situ stress on the excavation surface caused by the blasting excavation is a truly transient dynamic process, which differs from the quasi-static unloading (Field et al. 2004; Fan et al. 2015, 2016). Consequently, when the strain rate is lower than $10^{-1}/s$, then the effect of the inertial force can be ignored, and the unloading of the in situ stress caused by TBM excavation is a quasi-static process, which agrees with Barton (2000). In different unloading paths, dynamic effects caused by in situ stress unloading are quite different, and a longer unloading time can reduce the dynamic effect within a certain time range (Li et al. 2014). Therefore, the excavation response in the surrounding rock mass under blasting excavation and TBM excavation should be analyzed separately.

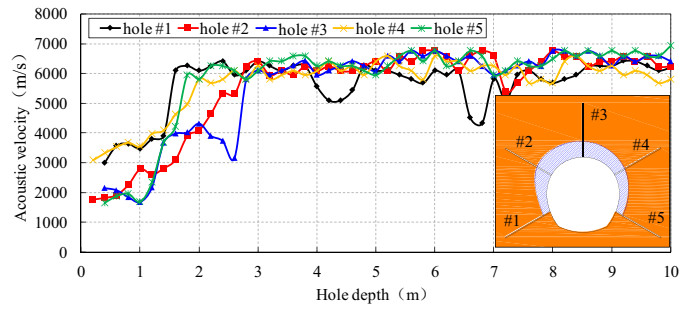
In practical engineering construction, the lateral pressure coefficient k is generally used to describe the stress state of a certain area. When the direction of the tunnel axis is consistent with the direction of the minimum horizontal in situ stress, the lateral pressure coefficient k is the ratio of the maximum horizontal principal stress to the vertical stress. When the direction of the tunnel axis is consistent with the direction of the

Table 2 Detection results for the detection sections in diversion tunnel 2[#]

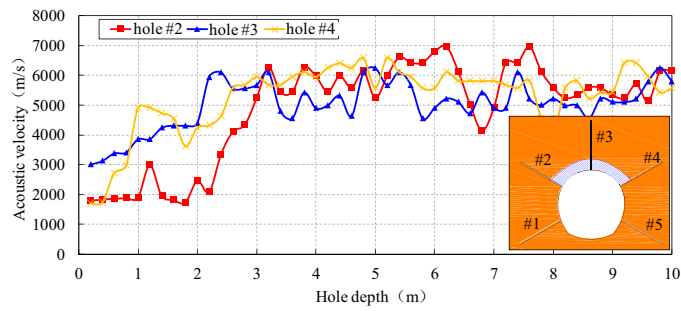
Positions of the detection sections	Lithology	Surrounding rock classification	Burial depth (m)	Hole #1	Hole #2	Hole #3	Hole #4	Hole #5	
Extents of damage zone (m)	K15700	T _{2y} ⁶	III	1054	2.8	2.8	3.6	4.2	3.0
	K15505	T _{2y} ⁵	II	1110	1.6	2.8	2.8	2	1.8
	K14500	T _{2y} ⁵	III	1637	—	2.8	2.2	2.6	—
	K14245	T _{2y} ⁵	II	1725	—	2.1	2.2	1.8	—
	K13880	T _{2y} ⁶	III	1840	—	1.8	2.2	3.6	—



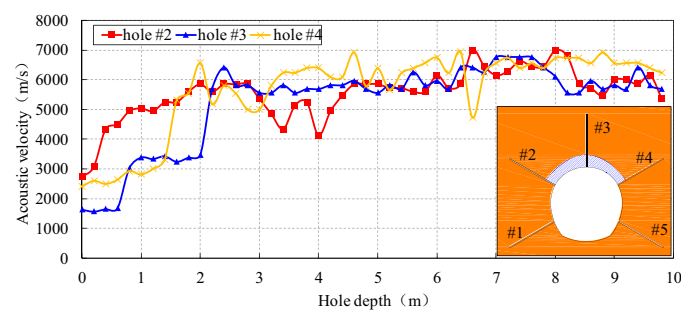
(a)



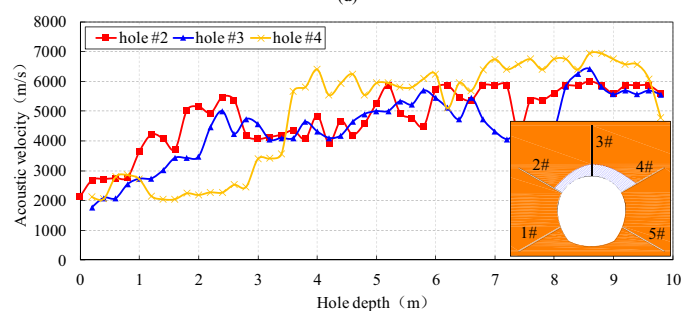
(b)



(c)



(d)



(e)

◀ **Fig. 11** Detection results for the detecting sections in the diversion tunnel 2#. **a** Section K15700. **b** Section K15505. **c** Section K14500. **d** Section K14245. **e** Section K13880

maximum horizontal in situ stress, the lateral pressure coefficient k is the ratio of the minimum horizontal principal stress to the vertical stress.

Assuming the blasting excavation of deep buried circular cavern in a hydrostatic stress field ($k = 1$), the tunnel section is formed by one-time blasting excavation with a radius of a , and the vertical compressive stress is P_0 , which belongs to a plane strain problem (Li et al. 2014; Zhu et al. 2014). Before excavation, the stress state of the surrounding rock mass on the proposed excavation boundary is shown in Fig. 14b, which can be counted by (Xu 2006):

$$\begin{cases} \sigma_r = \frac{P_0}{2}[(1+k) - (1-k)\cos(2\varphi)] \\ \sigma_\varphi = \frac{P_0}{2}[(1+k) + (1-k)\cos(2\varphi)] \\ \tau_{r\varphi} = \frac{P_0}{2}(1-k)\sin(2\varphi) \end{cases} \quad (2)$$

where σ_r is the radial stress; σ_φ is the tangential stress; $\tau_{r\varphi}$ is the shear stress; and φ is the inclination angle.

After calculating by Eq. (2), the excavation area is in the hydrostatic stress field P_0 . Before excavation, the constraint of the excavated rock mass on the surrounding rock mass is regarded as a reverse load acting on the excavation boundary, which is equal to the in situ stress. During blasting excavation, when the pressure induced by blasting on the excavation boundary decays to a level which is equal to the in situ stress P_0 , the transient unloading starts (Lu et al. 2012). Then, under the unloading action of the time-dependent tensile load $P(t)$, the in situ stress decreases rapidly from the initial value P_0 to 0 with 2 ms (Lu et al. 2012), resulting in transient unloading of the in situ stress. To simplify the calculations, the unloading of the in situ stress on the excavation surface Fig. 14a is formulated by superimposing the initial in situ stress state (Fig. 14b) and the unloading state (Fig. 14c), which is presented in Fig. 14 (Li et al. 2014; Zhu et al. 2014). After the treatments described above, the unloading of in situ stress is equivalent to the superposition of the initial stress and the dynamic tensile load on the excavation boundary. Based on the above analysis, the problem of in situ stress unloading can be further transformed into the problem of column cavity excitation; that is, in the beginning, a time-dependent tensile stress acts on the columnar cavity in the stress-free state.

In cylindrical coordinates, the dynamic stress field of the surrounding rock mass can be obtained by solving the following governing equation and superimposing the

initial in situ stress field. In the following equations, the compressive stress is positive, the tensile stress is negative, and the radius of the column cavity (excavation radius) is assumed as a .

Governing equation:

$$\begin{cases} \frac{\partial^2 u}{\partial r^2} + \frac{1}{r} \frac{\partial u}{\partial r} - \frac{u}{r^2} = \frac{1}{C_p^2} \frac{\partial^2 u}{\partial t^2} \\ \sigma_r(r, t) = (\lambda + 2\mu) \frac{\partial u}{\partial r} + \lambda \frac{u}{r} \\ \sigma_\varphi(r, t) = \lambda \frac{\partial u}{\partial r} + (\lambda + 2\mu) \frac{u}{r} \end{cases} \quad (3)$$

Boundary conditions:

$$u(r, t) = \frac{\partial u}{\partial t} = 0 (r \geq a, t < 0) \quad (4)$$

$$[\sigma_r]_{r=a} = \begin{cases} 0 (t \leq 0) \\ -\frac{P_0 t}{t_0} (0 < t \leq t_0) \\ -P_0 (t \geq t_0) \end{cases} \quad (5)$$

$$\lim_{r \rightarrow \infty} [u] = 0 \quad t > 0 \quad (6)$$

where λ and μ are the lame constants; $u(r, t)$, $\sigma_r(r, t)$, and $\sigma_\varphi(r, t)$ are the radial displacement, radial stress, and tangential stress induced by the transient unloading of the surrounding rock mass, respectively; C_p is the elastic longitudinal wave velocity (m/s); $C_p = \sqrt{(\lambda + 2\mu) / \rho}$; ρ is the density of the rock mass (kg/m³); t is time; t_0 is the duration of the transient unloading of the in situ stress; and r is the distance from the surrounding rock mass to the excavation center.

Figure 15 shows the dynamic stress field induced by the transient unloading of the in situ stress on the surrounding rock mass ($r = 2a$). In Fig. 15, the stress redistribution caused by the quasi-static unloading of the in situ stress is calculated using Eq. (7):

$$\left. \begin{aligned} \sigma_r &= P_0(1 - a^2/r^2) \\ \sigma_\varphi &= P_0(1 + a^2/r^2) \end{aligned} \right\} \quad (7)$$

During calculation, the in situ stress field P_0 is assumed as 20 MPa, the elastic longitudinal wave velocity C_p is 4500 m/s, the duration time of transient unloading t_0 is 2 ms, and the excavation radius a is 5.0 m.

As can be seen from Fig. 15, the transient unloading of the in situ stress on the excavation boundary causes the radial stress on the surrounding rock mass to unload and rebound rapidly, whereas the tangential stress is loading. In addition, the radial stress and the tangential stress on the surrounding rock mass initially decrease, then increase, and finally stabilize to the secondary stress value of quasi-static unloading.

Compared with the quasi-static unloading of in situ stress, transient unloading of in situ stress produces an additional dynamic stress, which increases the effects of the radial unloading and tangential loading effects on the surrounding rock mass and enlarges the difference between the radial stress and the tangential stress.

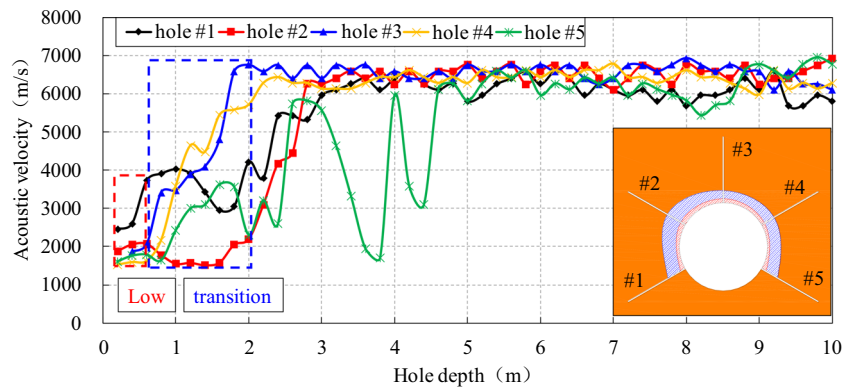
EDZ induced by transient unloading and quasi-static unloading

As analyzed in “In situ stress unloading caused by blasting excavation and TBM excavation”, it will cause a significantly different response of stress adjustment in the surrounding rock

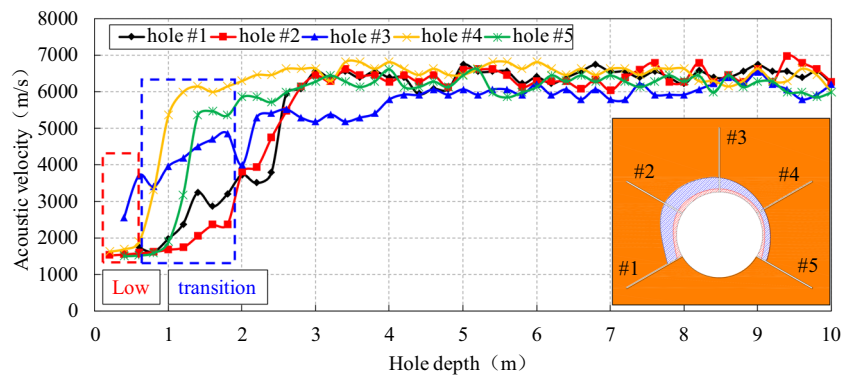
mass after the transient unloading of in situ stress and quasi-static unloading of in situ stress. According to the acoustic data analysis in “Acoustic detection results” and “Composition of EDZ,” the stress adjustment induced by the blasting excavation (transient unloading) and the TBM excavation (quasi-static unloading) plays a key role in the formation of EDZ. Thus, the EDZ caused by these two unloading paths is studied in this section.

This is because the Griffith criterion is convenient for theoretical calculation, and it not only reflects the effect of principal stress difference but also summarizes the characteristics of uniaxial stress states, triaxial stress states, and various combinations of the stress state such as compression and tension

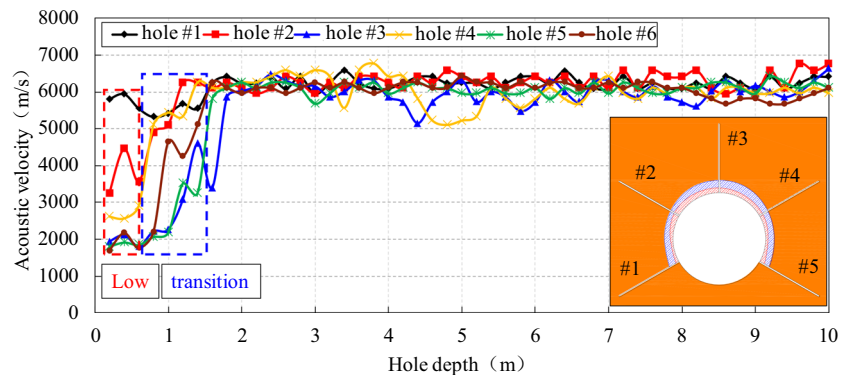
Fig. 12 Distribution of the low-velocity bands and transition velocity bands in the detection sections of diversion tunnel 1#. **a** Section K15700. **b** Section K15150. **c** Section K14280



(a)



(b)



(c)

when rock mass reaches tensile strength and fractures (Griffith 1921). Thus, the Griffith strength criterion is employed as the failure criterion in this section. According to the Griffith theory, stress concentration occurs around microcracks, especially at the ends of cracks, which is more likely to cause crack propagation and damage of the rock mass. The damage criterion is as follows:

$$\begin{cases} (\sigma_1^2 - \sigma_3^2) - 8\sigma_t(\sigma_1 + \sigma_3) = 0\sigma_1 + 3\sigma_3 > 0 \\ \sigma_3 = -\sigma_t\sigma_1 + 3\sigma_3 < 0 \end{cases} \quad (8)$$

where σ_1 is the maximum principal stress; σ_3 is the minimum principal stress; and σ_t is the tensile strength of the rock mass.

For the case presented in this paper, the Griffith theory can be simplified as follows:

$$m = (\sigma_1 - \sigma_3) / 8\sigma_t \quad (9)$$

When $m \geq 1$, the unloading disturbance has caused damage to the surrounding rock mass. While the tensile strength of the rock mass is obtained, the dynamic stress field ($\sigma_1 = \sigma_\varphi$, $\sigma_3 = \sigma_r$) shown in Fig. 15 can be input into Eq. (9) to determine whether the surrounding rock mass is damaged. The transient unloading of in situ stress increases the effects of the radial stress unloading and the tangential stress loading of the surrounding rock mass, resulting in an increase of the difference between the maximum principal stress and the minimum principal stress. Thus, the surrounding rock mass is more likely to be damaged during transient unloading. To show these characteristics more intuitively, Fig. 16 gives the extents of the EDZ caused by the transient unloading of in situ stress and the quasi-static unloading of in situ stress calculated by the simplified criterion.

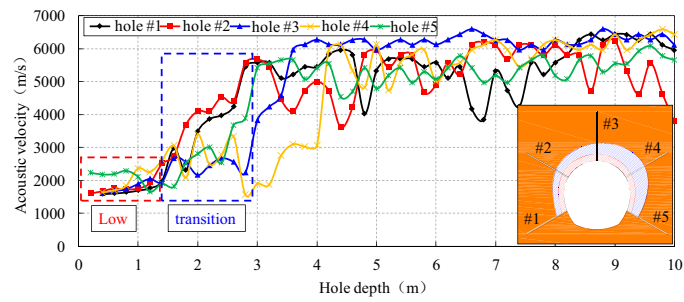
As can be seen from Fig. 16, the extent of the EDZ caused by the transient unloading of in situ stress is about $0.7a$, and

the extent of the EDZ induced by the quasi-static unloading of in situ stress is about $0.6a$. This indicates that under high in situ stress conditions, transient unloading increases the effects of the radial stress unloading and the tangential stress loading of the surrounding rock mass and results in more damage to the surrounding rock mass. In this paper, the in situ stress value adopted in the calculation is 20 MPa, while the in situ stress magnitude of the Jinping II hydropower diversion tunnel reaches 50–70 MPa. It can be predicted that with the increase of in situ stress, the damage range of the surrounding rock mass caused by transient unloading of in situ stress during blasting excavation will be larger. To prove this, the measured data of EDZ will be analyzed in the following sections.

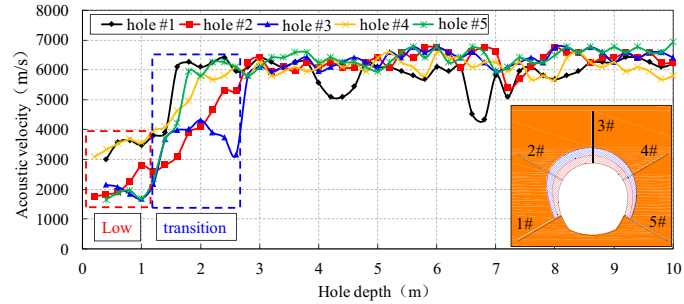
When the lateral pressure coefficient of excavation area is not equal to 1. The excavation area is in a non-hydrostatic stress field due to the influence of structural stress and other factors. Therefore, the dynamic stress field and the extents of the EDZ induced by transient unloading of the surrounding rock mass cannot be obtained as easily as the case of the hydrostatic stress field. Thus, a numerical simulation method was conducted. Because FLAC3D adopts the algorithm of explicit finite difference, it can more realistically simulate the transient unloading process of in situ stress and the stress path of the surrounding rock mass during blasting excavation. Therefore, FLAC3D was employed to analyze the distribution of the EDZ induced by the transient unloading of in situ stress. During the simulation of transient unloading effect, it is assumed that the tunnel is formed by one-time excavation; the transient unloading effect of in situ stress on the excavation surface was accomplished by removing the elements of excavated area and inducing the dynamic stress field in the surrounding rock mass. While employing FLAC3D to simulate quasi-static unloading, it needs to take a special simulation program: firstly, the elastic model was adopted for calculation

Table 3 Detection data partition for diversion tunnel 1[#]

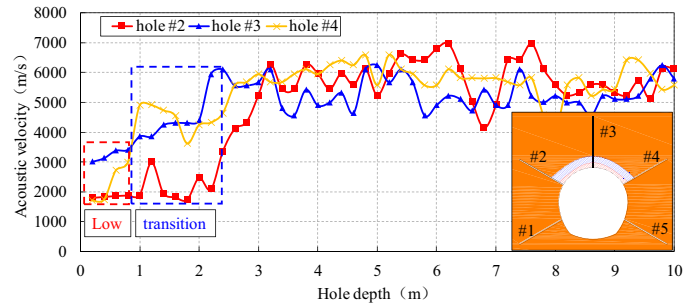
Position of test section	Surrounding rock classification	Burial depth (m)	Hole #1	Hole #2	Hole #3	Hole #4	Hole #5
Depths of low velocity bands (m)	K15700 II	1092	0.80	0.70	0.60	0.50	0.80
	K15150 III	1400	0.90	0.75	0.50	0.40	0.80
	K14280 III	1750	0.50	0.80	0.70	0.40	0.80
Depths of transition velocity bands (m)	K15700 II	1092	2.20	2.10	1.20	1.70	2.00
	K15150 III	1400	1.70	2.05	1.70	0.80	0.60
	K14280 III	1750	1.10	0.40	1.10	1.00	0.80
Depth of low velocity bands/depth of transition velocity bands	K15700 II	1092	0.36	0.33	0.50	0.29	0.40
	K15150 III	1400	0.53	0.37	0.29	0.50	1.33
	K14280 III	1750	0.45	2.00	0.64	0.40	1.00
The percentage of the low velocity band in the total damage zone	K15700 II	1092	27%	25%	33%	23%	29%
	K15150 III	1400	35%	27%	23%	33%	57%
	K14280 III	1750	31%	67%	39%	29%	50%



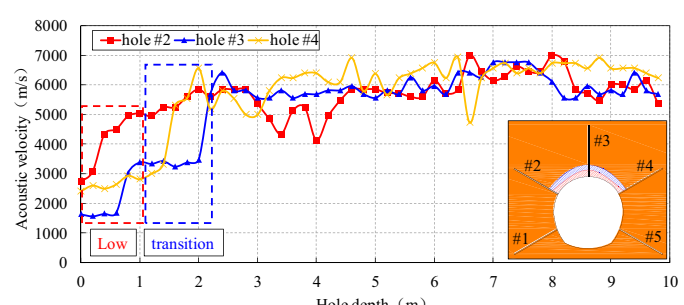
(a)



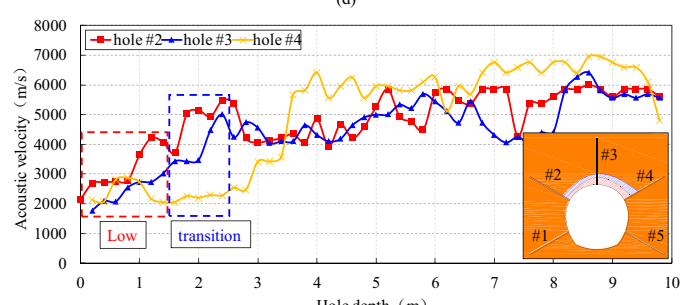
(b)



(c)



(d)



(e)

◀ **Fig. 13** Distribution of the low-velocity bands and transition velocity bands in the detection sections of diversion tunnel 2[#]. **a** Section K15700. **b** Section K15505. **c** Section K14500. **d** Section K14245. **e** Section K13880

during simulation of excavation; after obtaining the elastic solution, the surrounding rock material was replaced with the elastoplastic constitution; finally, the calculations were run continuously until the balance was achieved. In this way, the effect of transient stress unloading can be avoided, and the stress adjustment process induced by quasi-static unloading can be simulated. This treatment can be summarized into two steps: elastic excavation and plastic balance (Cai 2007).

The mechanical parameters obtained from an underground experiment (granite) conducted by the URL in Canada were used (Table 7) for the numerical simulation. Assuming a circular section with a diameter of 3.5 m and a horizontal initial in situ stress of 60 MPa, the value of the lateral pressure coefficient k was adjusted by reducing the vertical in situ stress.

The Mohr-Coulomb strength criterion was employed to analyze the extents of the EDZ. The left side of Fig. 17 shows the extents of the EDZ caused by the transient unloading of in situ stress (blasting excavation) for a lateral pressure

coefficient of 2, 3, 4, 5, and 5.5. For comparison, the method of elastic excavation and plastic balance was used to simulate the extents of the EDZ induced by the quasi-static unloading of in situ stress (TBM excavation) under the same conditions (right side of Fig. 17). Based on the theoretical calculation results shown in Fig. 15, excavation and unloading result in the radial stress unloading and tangential stress loading of the surrounding rock mass, which change the stress path of the surrounding rock mass. During the stress loading and unloading process, when the rock unit reaches the yield state (shear-n, tension-n), the process will not stop, and the rock unit may change into the shear-p or tension-p state. Therefore, the shear-n, tension-n, shear-p, and tension-p states shown in Fig. 17 all indicate that the surrounding rock mass has been damaged.

As can be seen from Fig. 17, when $k = 2$, for quasi-static unloading, shear damage zones only occur at the top and bottom of the surrounding rock mass, whereas for transient unloading, tensile damage zones occur around the excavation contour. Moreover, as the lateral pressure coefficient increases, the extents of the EDZ of the surrounding rock mass caused by TBM excavation and blasting excavation increase. The shear damage zones mainly occur at the top and bottom of the surrounding rock mass (the direction of the minimum principal stress), and the tensile damage zones mainly take place at the sides of the surrounding rock mass (the direction

Table 4 Detection data partition for diversion tunnel 2[#]

Position of test section		Surrounding rock classification	Burial depth (m)	Hole #1	Hole #2	Hole #3	Hole #4	Hole #5
Depths of low velocity bands (m)	K15700	III	1054	1.60	1.40	1.40	1.20	1.30
	K15505	II	1110	1.10	1.60	1.40	1.10	1.30
	K14500	III	1637	—	1.00	0.90	1.10	—
	K14245	II	1725	—	1.40	1.20	1.20	—
	K13880	III	1840	—	1.00	1.50	1.80	—
Depths of transition velocity bands (m)	K15700	III	1054	1.20	1.40	2.20	3.00	1.70
	K15505	II	1110	0.50	1.20	1.40	0.90	0.50
	K14500	III	1637	—	1.80	1.30	1.50	—
	K14245	II	1725	—	0.70	1.00	0.60	—
	K13880	III	1840	—	0.80	0.70	1.80	—
Depth of low velocity bands/depth of transition velocity bands	K15700	III	1054	1.33	1.00	0.64	0.40	0.76
	K15505	II	1110	2.20	1.33	1.00	1.22	2.60
	K14500	III	1637	—	0.56	0.69	0.73	—
	K14245	II	1725	—	2.00	1.20	2.00	—
	K13880	III	1840	—	1.25	2.14	1.00	—
The percentage of the low velocity band in the total damage zone	K15700	III	1054	57%	50%	39%	29%	43%
	K15505	II	1110	69%	57%	50%	55%	72%
	K14500	III	1637	—	36%	41%	42%	—
	K14245	II	1725	—	67%	55%	67%	—
	K13880	III	1840	—	56%	68%	50%	—

Table 5 Thrust and tunneling rate of the TBM excavation of the Jinping construction drainage tunnel

Date	Shift	Excavation termination station (m)	Propulsion pressure (PSI)	Tunneling rate (m/h)	Classification of surrounding rock
2009-5-11	Day shift	SK10 + 803.592	900–1000	\	II/III
	Night shift	SK10 + 793.037	1000–2800	2.5	II/III
2009-5-12	Day shift	SK10 + 777.182	2300–2800	2.6	II
	Night shift	SK10 + 762.511	1200–3000	2.88	II
2009-5-13	Day shift	SK10 + 753.867	900–2000	3.02	II
	Night shift	SK10 + 734.952	2900–3000	2.85	II
2009-5-14	Day shift	SK10 + 720.904	1500–3000	3.2	II
	Night shift	SK10 + 704.964	1800–3000	3	II
2009-5-15	Day shift	SK10 + 686.900	2800–3000	2.4	II
	Night shift	SK10 + 669.793	1000–3000	2.9	II
2009-5-23	Day shift	SK10 + 529.975	900–2400	2.4	III
	Night shift	SK10 + 513.920	1000–3000	2.7	III
2009-5-24	Day shift	SK10 + 502.680	1000–1600	2.5	III
	Night shift	SK10 + 488.250	1000–2700	2.6	III
2009-5-25	Day shift	SK10 + 478.462	900–2800	2.8	III
	Night shift	SK10 + 488.252	2200–2800	2.8	III

of maximum principal stress). Compared with transient unloading, the quasi-static unloading does not cause EDZ around the excavation contour in the upper left side, lower left side, upper right side, and lower right side of the excavation boundary, while transient unloading causes more EDZs around the excavation boundary. This illustrates that transient unloading tends to cause damage to the rock mass around the

excavation contour, and it is also in accordance with the acoustic data that a larger severe damage zone (low velocity band) is formed around the excavation contour induced by transient unloading (blasting excavation). The reason is that the transient unloading of in situ stress causes radial stress unloading and tangential stress loading effects in the

Table 6 Strain rates induced by blasting excavation and TBM excavation

Excavation method	In situ stress	Duration time of in situ stress unloading	Strain rate (s^{-1})
Blasting excavation	20–50 MPa	2–5 ms	10^{-1} – 10^1
TBM excavation		>24 ms	$<10^{-2}$

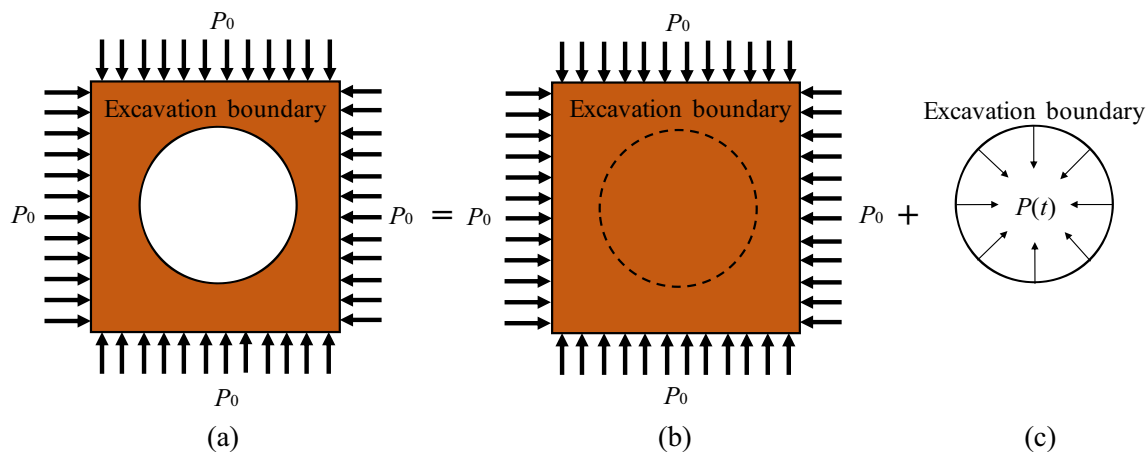
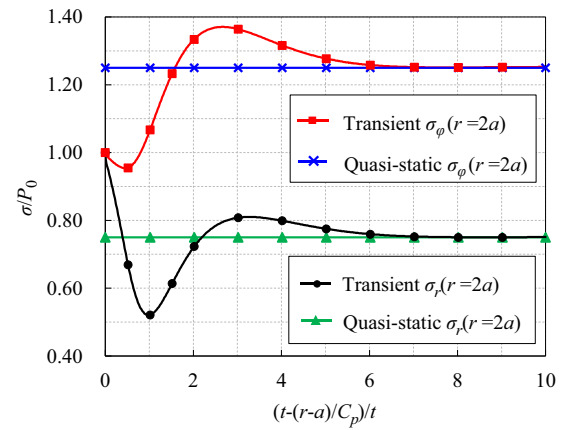
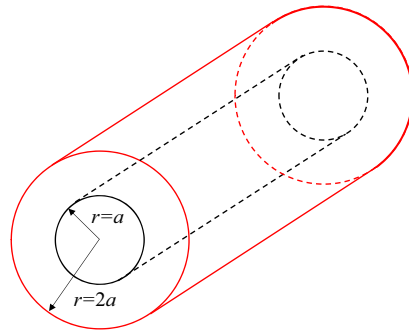


Fig. 14 Mechanical model of transient stress unloading for a deep circular tunnel. **a** Transient unloading of in situ stress. **b** Initial stress state. **c** Unloading state

Fig. 15 Dynamic stress induced by the transient unloading of the in situ stress



surrounding rock mass, which makes the rock mass around the tunnel more prone to tensile or shear damage.

Figure 18 shows the damage zone in the surrounding rock mass (granite) induced by the non-explosive (mechanical) excavation in the URL (Read 2004). The results of acoustic emission and microseismic monitoring show that the compression shear damage occurs in the direction of the minimum principal stress (σ_3), and a large area of the tensile damage occurs in the direction of the maximum principal stress (σ_1). Excluding the influence of the direction of the in situ stress field, the damage zone in the surrounding rock mass caused by the quasi-static stress unloading (TBM excavation) simulated using

FLAC3D (Fig. 17) is consistent with the measured results of Read (2004), which verifies the correctness of the numerical simulation method employed in this paper.

Numerical simulation of EDZ at Jinping II diversion tunnels

Mechanical properties of the Jinping marble

The main lithology exposed during the excavation of the diversion tunnels of the Jinping II hydropower project is marble.

Fig. 16 Extents of the damage caused by transient and quasi-static unloading

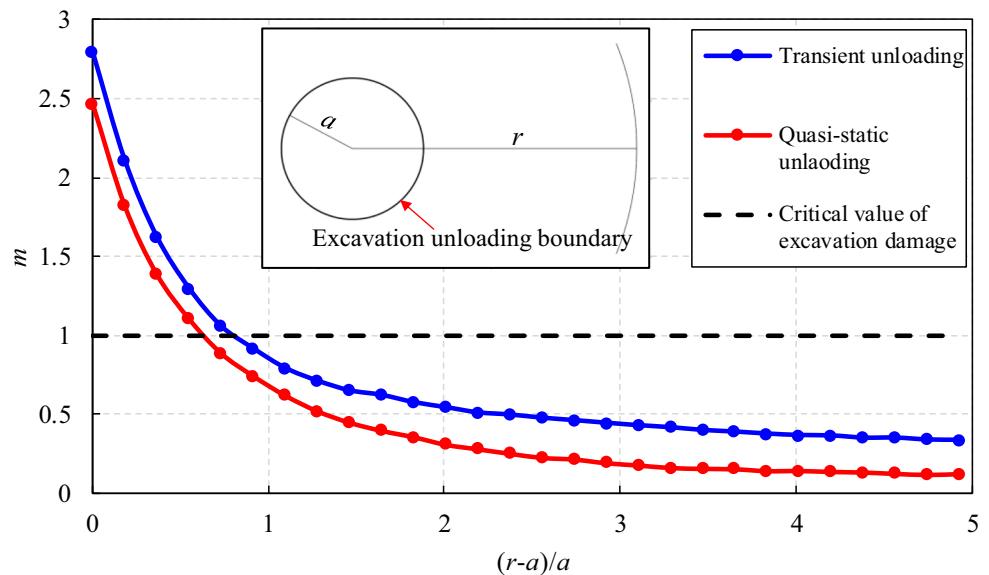
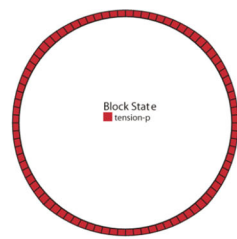
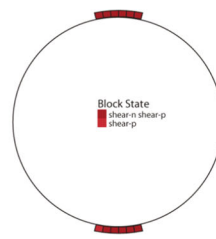


Table 7 Rock mass parameters from an underground experiment (granite) conducted by the URL

Compressive strength	Tensile strength	Shear strength	Internal cohesion
128 MPa	3.7 MPa	6 MPa	25 MPa
Friction angle	Elastic modulus	Poisson ratio	Axial stress
48°	60 GPa	0.2	45 MPa

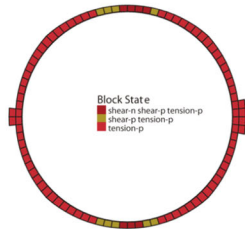


Transient unloading

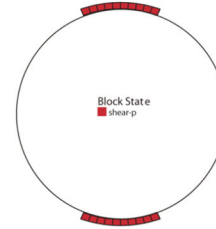


Quasi-static unloading

(a)

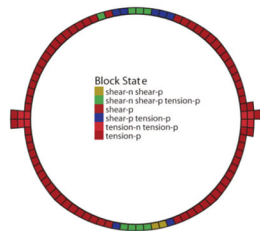


Transient unloading

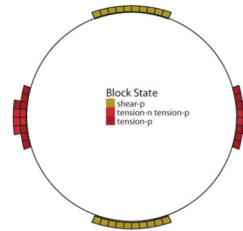


Quasi-static unloading

(b)

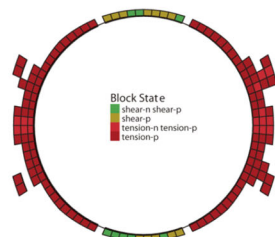


Transient unloading

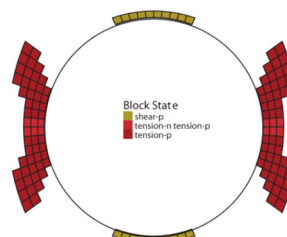


Quasi-static unloading

(c)

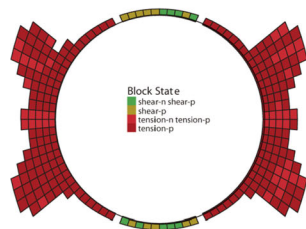


Transient unloading

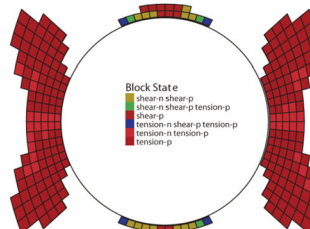


Quasi-static unloading

(d)



Transient unloading



Quasi-static unloading

(e)

◀ **Fig. 17** Distributions of the EDZ caused by transient and quasi-static unloading. **a** $k = 2$. **b** $k = 3$. **c** $k = 4$. **d** $k = 5$. **e** $k = 5.5$

Therefore, it is crucial to analyze the post-peak mechanical property of the Jinping marble before numerically simulating the damage to surrounding rock mass induced by tunnel excavation. Previous studies have shown that the stress-strain characteristics and yield forms of marble are closely associated with the confining pressure. When the confining pressure is low, the mechanical property of the rock mass is mainly brittle, and the stress-strain curve of the marble rapidly decreases after reaching the peak strength. Then, as the confining pressure level increases, the ductility characteristic of the marble gradually appears. Finally, while the confining pressure increases to a certain level, the stress-strain curve of marble does not decrease and the residual strength does not reduce after reaching the peak strength, that is, the plastic characteristics. Thus, the mechanical properties of the Jinping marble are associated with the confining pressure of the rock mass, which can be described as brittle-ductile-plastic transition characteristics (Wawersik and Fairhurst 1970). To further explore the mechanical properties of the Jinping marble, Chu (2009) conducted borehole sampling at burial depths of more than 2000 m in the eastern end of the Jinping transportation tunnel, the sample lithology is Baishan group marble, and the results of triaxial compression tests conducted on the sample are shown in Fig. 19.

As can be seen from Fig. 19, when the confining pressure is between 2 and 8 MPa, the sample presents obvious ductility characteristics, and the brittle characteristics are still observed

at a confining pressure of 2 MPa. When the confining pressure increases to 40 MPa, the sample shows perfectly plastic characteristics within 1% of the axial strain level. This result is consistent with the research results of Wawersik and Fairhurst (1970), as shown in Fig. 20.

From Fig. 20, as the confining pressure increases, the marble exhibits the mechanical characteristics of the brittle-ductile-plastic transition, and the level of confining pressure is not high when the transition occurs. The brittle-ductile transition occurs within a few megapascals of the confining pressure, and the confining pressure of the ductile-plastic transition is about 40 MPa. According to the engineering data provided above, the confining pressure of the deeply buried tunnels of the Jinping II hydropower project can easily reach the condition of brittle-ductile-plastic transition. Therefore, even if the rock mass is undamaged, different parts of the surrounding rock mass will exhibit different mechanical properties after excavation. The above analyses fully demonstrate that analyzing and mastering the mechanical characteristics of marble are of great significance to the further investigation of the excavation response of the deeply buried tunnels of the Jinping II hydropower project.

Determination of the constitutive model and calculation parameters

In order to analyze the influences of the different excavation methods on the distribution of the excavation damage zone in the diversion tunnels of the Jinping II hydropower project, the excavation responses caused by TBM excavation and blasting

Fig. 18 Damage zones caused by machine excavation in the URL ($\sigma_1 = 60$ MPa, $\sigma_3 = 11$ MPa) (Read 2004)

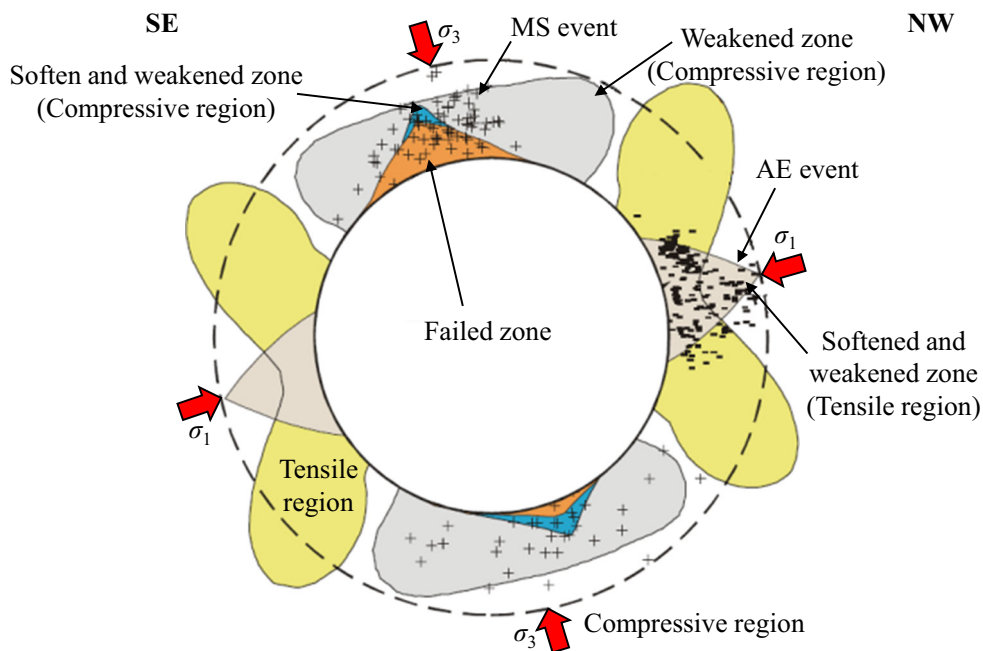
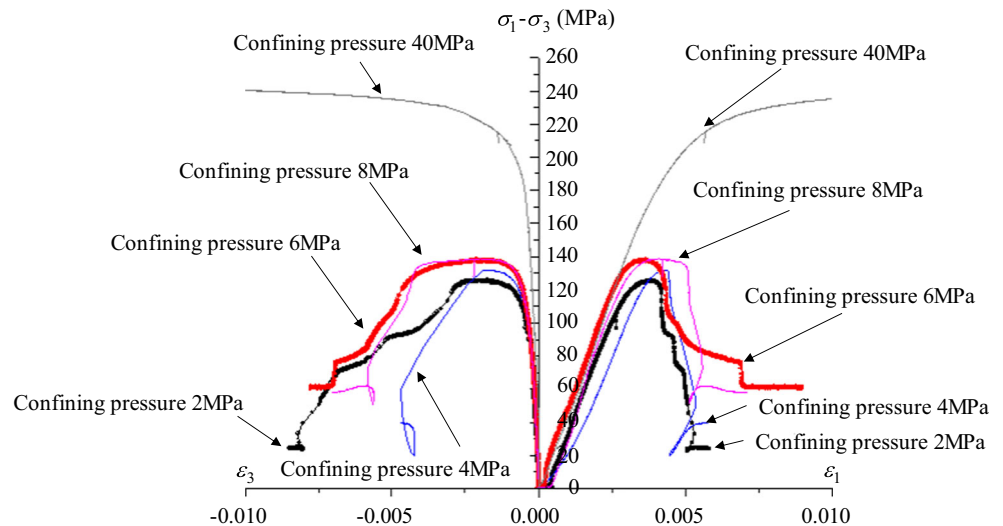


Fig. 19 Triaxial compression test results for the Jinping Baishan Group marble (Chu 2009)



excavation were numerically simulated. Before the numerical simulation, it is crucial to determine the numerical description method for the mechanical properties of the brittle-ductile-plastic transition of the Jinping marble. However, the strength criterion used above cannot take into account the special mechanical properties of Jinping marble, so other strength criteria need to be adopted in numerical simulation. Because the strength parameters m_b , s , and a in the Hoek-Brown strength criterion equation (Eq. (10)) can change with the accumulation of plastic strain ϵ_3^p after rock mass yielding, the Hoek-Brown strength criterion was adopted to describe the strengthening and softening behavior of the material after yielding (Cundall et al. 2003).

$$\sigma_1 = \sigma_3 + \sigma_c \left(m_b \frac{\sigma_3}{\sigma_c} + s \right)^a \quad (10)$$

where m_b , s , and a are the parameters associated with the rock mass quality GSI and the rock mass material parameter m_i .

In order to accurately describe the changes in m_b , s , a and other parameters with the accumulation of plastic

strain under different confining pressures, Cundall et al. (2003) introduced a scaling factor μ_1 , which is related to the minimum principal stress, and the value of μ_1 can be adjusted for different confining pressures in the numerical calculation to describe the mechanical properties of the brittle-ductile-plastic transition of the marble. Because the environment of the surrounding rock mass and the stress paths reproduced by the indoor test are different from the real environment of the surrounding rock mass and the stress paths in the practical engineering, hence, the Hoek-Brown criterion was used to describe the mechanical characteristics of the brittle-ductile-plastic transition of the Jinping marble by employing the method of mutual verification of numerical tests and field damage detection (Zhang et al. 2010). First, several working conditions were assumed; that is, different scaling factors μ_1 were set to adjust the brittle-ductile-plastic transition of the marble under a certain confining pressure. Then, the stress path induced by the excavation of the different working conditions was calculated. If the low stress distribution zone is consistent with the EDZ extents of the surrounding rock mass obtained from field acoustic tests, it means the assumed working condition is correct.

Due to the troublesome determination process, in this paper, only one of the assumed working conditions was described: when the confining pressure is 0–2 MPa, the marble exhibits brittle characteristics, and when the confining pressure increases to 16 MPa, the ductile-plastic transition occurs. The Hoek-Brown mechanical parameters and the in situ stress field of section K15505 are used for the numerical simulation inversion. As shown in Table 8, σ_{xx} is the horizontal in situ stress field; σ_{zz} is the vertical in situ stress field; σ_{yy} is the tunnel axial in situ stress field; and GSI , m_i , m_b , s , and a are the Hoek-

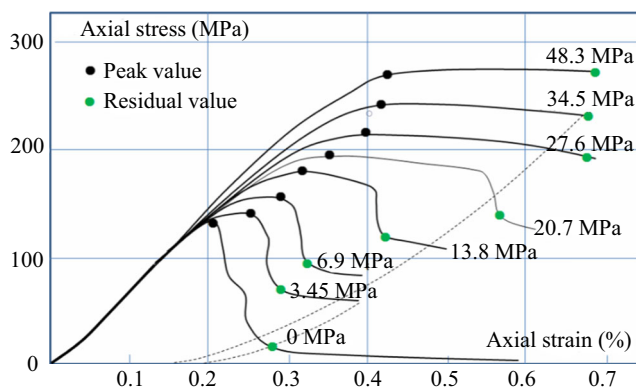


Fig. 20 Experimental results of the basic mechanical properties of marble (Wawersik and Fairhurst 1970)

Table 8 Hoek-Brown mechanical parameters and in situ stress field of section K15505

Compressive strength	Elastic modulus	GSI	m_i	m_b	s	a
140 MPa	36.1 GPa	70	9	3.0827	0.0357	0.5
Tensile strength	σ_{xx}	σ_{yy}	σ_{zz}	σ_{xy}	σ_{xz}	σ_{yz}
1.6 MPa	43.9 MPa	50.8 MPa	38.5 MPa	2.4 MPa	-3.0 MPa	3.6 MPa

Brown parameters. The parameters of the assumed working conditions are shown in Tables 9 and 10. According to the above parameters, a square model $1\text{ m} \times 1\text{ m} \times 1\text{ m}$ (Fig. 21) was established, and then, we fixed the confining pressure and applied axial loading until the element is damaged. Finally, by changing the confining pressure and repeating the above loading process, the axial stress-strain curves of the element for different confining pressures are obtained (Fig. 21).

According to the stress-strain curve in Fig. 21, the mechanical characteristics of the rock mass are mainly brittle under the low confining pressure. With the increase of confining pressure, the ductile characteristics of the rock mass gradually occur. Finally, when the confining pressure reaches 16 MPa, the rock mass exhibits plastic characteristics. After successfully describing the post-peak mechanical properties of the marble, a corresponding model was established according to the size and shape of the excavation section of diversion tunnel 2[#] (Fig. 7), and the low stress distribution zones caused by the transient unloading of in situ stress were calculated adopting the parameters in Tables 8, 9, and 10. Then, taking the surrounding rock mass with an angle of 30° to the x -axis (hole #4) as an example, the stress paths of the surrounding rock mass with 1 m, 1.5 m, 2 m, 2.5 m, and 3 m away from the

excavation surface were recorded from the numerical calculations (Fig. 22). In Fig. 22, when the stress path reaches the peak strength envelope, the rock mass is damaged. The more drastically the stress path drops, the more severely the surrounding rock mass is damaged. As can be seen from Fig. 22, blasting excavation causes transient unloading of the in situ stress on the excavation surface, which leads to dynamic unloading of the minimum principal stress (σ_3) and dynamic loading of the maximum principal stress (σ_1). This simulation result is consistent with that of previous theoretical calculations, which again demonstrates that FLAC3D can be employed to simulate the dynamic stress state of the rock mass during the transient unloading of in situ stress. Besides, as can be seen from Fig. 22, the stress paths of the surrounding rock mass at the monitoring locations with 1.0 m and 1.5 m away from the excavation surface decrease significantly after reaching the yield stress condition (peak strength envelope). The stress path curve of the surrounding rock mass located 2.0 m from the excavation surface does not decrease when it intersects with the peak strength envelope. Thus, the damage depth of the monitoring location is about 2.0 m, which is consistent with the damage extent of hole #4 in the surrounding rock mass of section K15505, which was previously determined by the acoustic detection method. Therefore, it is

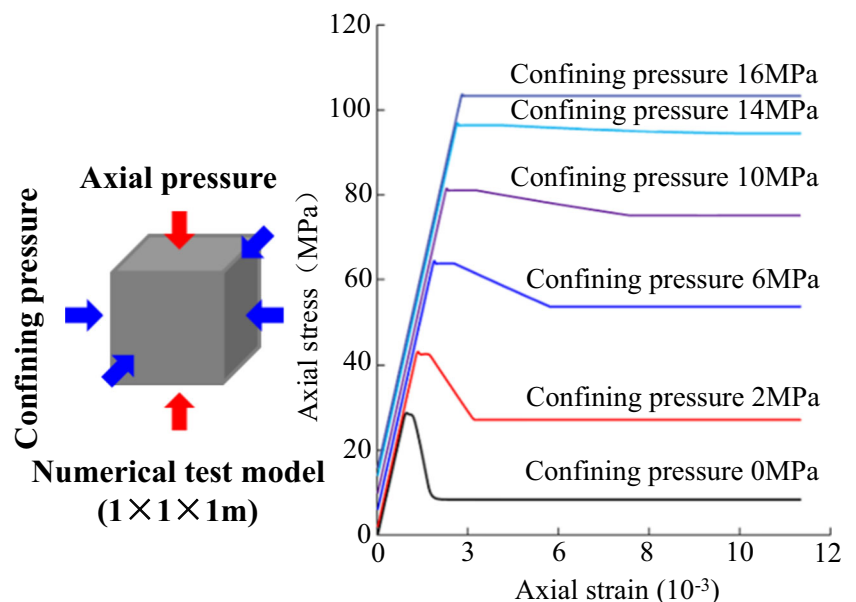
Fig. 21 Numerical inversion stress-strain curves of the marble

Table 9 Strength parameters of marble varying with plastic strain

Characteristic description	$\varepsilon_3^p / 10^{-3}$	σ_c (MPa)	m_b	s	a
Peak strength	0.00	140	3.0827	0.0357	0.50
Ductile section	1.20	140	3.0827	0.0357	0.50
Residual strength	2.30	140	4.1200	0	0.63

reasonable to use the parameters of Tables 9 and 10 to describe the brittle-ductile-plastic transition property of the Jinping marble.

Numerical simulation of EDZ induced by transient unloading and quasi-static unloading of in situ stress

According to Fig. 7, a corresponding model was established employing the parameters of “Determination of the constitutive model and calculation parameters.” Then, the excavation damage caused by the blasting excavation of section K15505 in diversion tunnel 2[#] was simulated in FLAC3D. The numerical simulation does not consider the explosive load and the effects of the relevant structural plane. First, the ideal elastic constitutive model was used to calculate the original stress field of the rock mass before excavation under the initial in situ stress, and the balance was obtained after a certain time step. Then, the parameters of Tables 8, 9, and 10 and the brittle-ductile-plastic mechanical transition model were employed to simulate the EDZ caused by the blasting excavation (Fig. 23).

As can be seen from Fig. 23, the numerical simulation results are consistent with the detection results, which further demonstrates the correctness of the analysis method and the calculation model used in this study. To further analyze the influence of the excavation unloading method on the distribution of the excavation damage zone, a model of the quasi-static unloading of in situ stress was established using the same parameters. The shape of the excavation surface in the model was consistent with the excavation section in diversion tunnel 1[#], and the calculation results are shown in Fig. 24.

As can be seen in Fig. 24, for blasting excavation, due to the dynamic effect caused by the transient unloading of the in situ stress, it causes larger damage zones at the bottom, the left side, and the right upper arch of the excavation boundary compared with the simulation result of

quasi-static unloading, and the maximum depth of the damage zone in the surrounding rock mass is about 3.3 m, while for quasi-static unloading, the maximum depth of damage zone in the surrounding rock mass caused by the quasi-static unloading of the in-situ stress is about 2.7 m. According to the analysis of testing data in “Composition of EDZ,” the damage caused by transient unloading is severer than that caused by quasi-static unloading according. Thus, more attention should be paid to the EDZ caused by transient unloading, although this part is not reflected in the numerical simulation.

After verifying the accuracy of the numerical simulation, the influence of the in situ stress direction on the excavation damage zone was simulated by adjusting the in situ stress direction in the model. The adjustment scheme is maintaining the original in situ stress and rotating the excavation section of the original model horizontally by 90°; the calculation results are shown in Fig. 25.

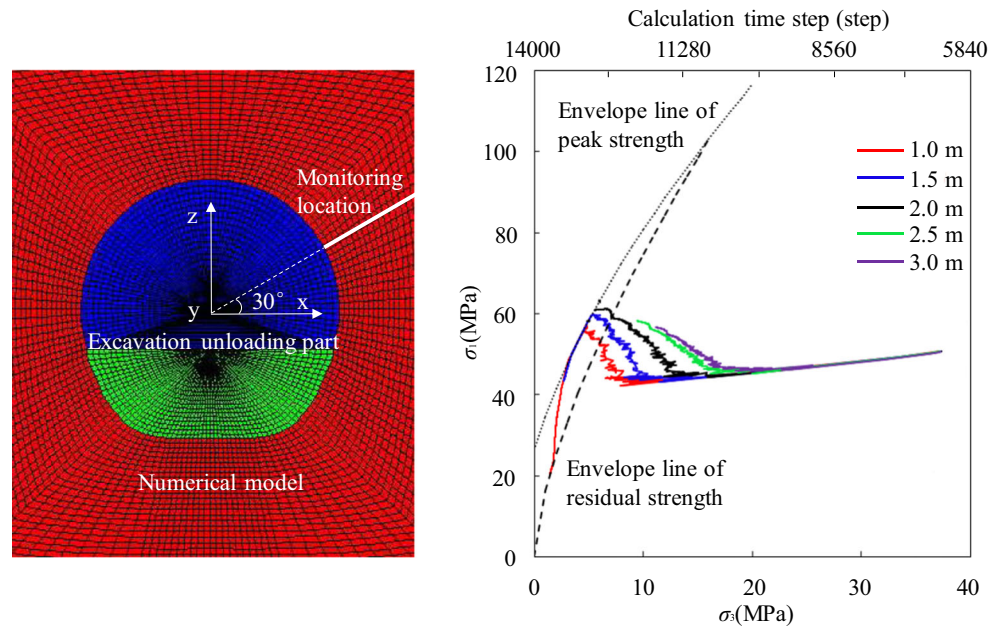
As can be seen from Figs. 24 and 25, when the maximum principal in situ stress is perpendicular to the tunnel axis, the EDZ extents calculated by using the current model are significantly larger than those calculated by adopting the original model. Moreover, the maximum damage zone in the surrounding rock mass occurs in the upper left arch and the bottom of the excavation section. Thus, we can conclude that the direction of the in situ stress also plays a significant role in the formation of the EDZ in the surrounding rock mass. When the maximum principal stress is perpendicular to the tunnel axis or has a large intersection angle to the tunnel axis, the surrounding rock mass is more likely to be damaged after excavation. After analyzing the influence of the in situ stress direction on the distribution of the EDZ through numerical simulations, the influences of the value of the in situ stress on the distribution of the EDZ (using the original in situ stress and increasing the confining pressure by 10 MPa) are also simulated; the simulation results are shown in Fig. 26.

As can be seen from Figs. 24 and 26, with the in situ stress increasing, the EDZ around the tunnel wall increases significantly, which coincides with the conclusion in “Composition of EDZ” that the larger the in situ stress, the more severely the surrounding rock mass will be damaged (the larger depths of the low-velocity band) after excavation. The simulation

Table 10 Scaling factor μ_1 related to the minimum principal stress σ_3

σ_3 (MPa)	0	2	4	8	12	15.9	16
μ_1	1.00	0.75	0.65	0.55	0.45	0.35	0

Fig. 22 Stress paths of the surrounding rock mass induced by excavation



results above all indicate the importance of in situ stress unloading induced by excavation to the EDZ.

Conclusions

The conclusions of this study are as follows:

- (1) In the process of deep tunnel excavation, there is a significant difference between the effects of blasting excavation and TBM excavation. The dynamic effects caused by the transient unloading of in situ stress during blasting excavation play an important role in the formation of the excavation damage zone. Compared with the quasi-static unloading of in situ stress, the transient unloading of in situ stress causes an additional dynamic stress in the surrounding rock mass, which enlarges the effects of the radial stress unloading and the tangential stress loading, and leads to the surrounding rock mass more likely to be damaged. As the lateral pressure coefficient increases, the extents of the damage of the surrounding rock mass induced by the transient unloading of in situ stress and the quasi-static unloading of in situ stress increase.
- (2) The acoustic detection results show that the damage zones in the surrounding rock mass caused by blasting excavation (K15700 2.8–4.2 m, K14500 2.2–2.8 m) are significantly larger than those caused by TBM excavation (K15700 1.8–3.0 m, K14280 1.2–1.8 m) under similar working conditions. It further demonstrates that the transient unloading of in situ stress aggravates the damage to the surrounding rock mass.
- (3) The EDZ of the Jinping deeply buried tunnel can be divided into the low-velocity band and the transition velocity band. The former is characterized by a significant decrease in the acoustic velocity; the surrounding rock mass in this region is severely damaged, so it basically loses its bearing capacity. The latter is characterized by a slow decrease in the acoustic velocity, and with the

Fig. 23 Comparison between the numerical simulation results and the EDZ detection results

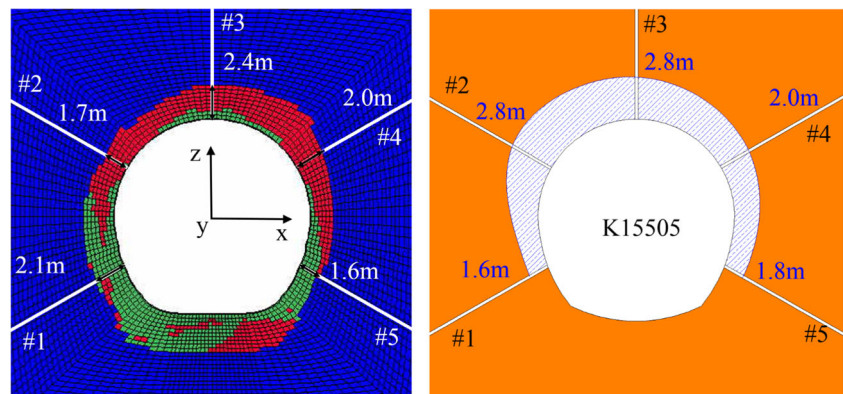
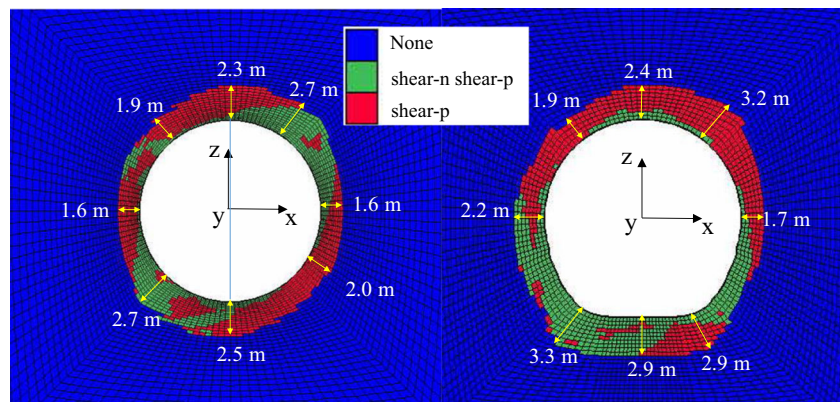


Fig. 24 Damage zones in the surrounding rock mass for different unloading paths of in situ stress



increase of depth, the acoustic velocity gradually recovers to the value of the undisturbed surrounding rock mass. During TBM excavation, the acoustic velocity of the rock mass in the damage zone transits smoothly from the excavation surface into the surrounding rock mass. However, during blasting excavation, the transition is significantly slower, and there are obviously low-velocity bands along the excavation contour, which indicates that the dynamic effects induced by the transient unloading of in situ stress have a significant influence on the formation of the damage zone. Furthermore, the low-velocity band is more likely to form in the class II surrounding rock mass after blasting excavation.

- (4) The depths of the low-velocity band measured in diversion tunnel 2[#] are significantly larger than those of the transition velocity band, and the distribution of the low-velocity band in the tunnel section is affected by the secondary stress field. It illustrates that the transient unloading of in situ stress caused by blasting excavation is one of the direct causes to the formation of the low-velocity band. In the detection section of blasting excavation, the depths of the low-velocity band account for 29–72% (mainly more than 50%) of the total depths of the damage zone, while in the detection section of the TBM excavation, the depths of the low-velocity band

- account for 23–57% (mainly 30%) of the total depths of the damage zone.
- (5) As the in situ stress increased, the proportions of the low-velocity band in diversion tunnel 1[#] increase from 27–29% to 31–67%, and the proportions of the low-velocity band in diversion tunnel 2[#] increase from 29–50% to 50–68%. This indicates that in situ stress has an important impact on the formation of the low-velocity band of the surrounding rock mass.
- (6) By considering the brittle-ductile-plastic transformation characteristics of the Jinping marble, the extents of the excavation damage zone of the surrounding rock mass for different excavation methods can be accurately estimated employing the numerical calculation method.

The work presented in this research only revealed the influence of the unloading mode of in situ stress and in situ stress field on the EDZ distribution. Blasting load, support, damage degree, impact induced by construction procedure, and complex geological conditions such as structural planes, faults, and fractures were not considered in the numerical simulation. Therefore, further studies on investigation of the distribution and evolution regularity of EDZ under more complete conditions will be performed in future work.

Fig. 25 Numerical simulation results of the EDZ after adjusting the direction of the in situ stress

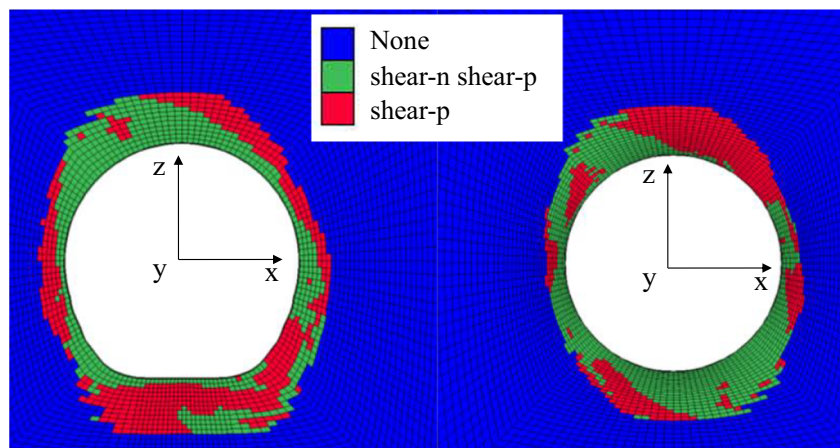
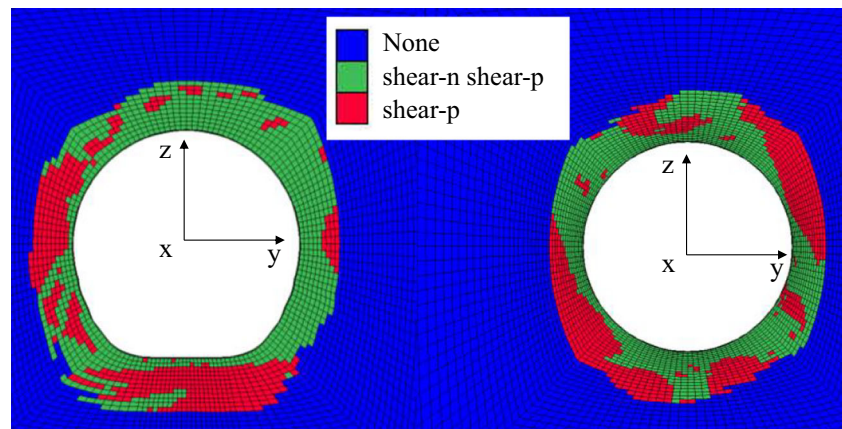


Fig. 26 Numerical simulation results of the EDZ after adjusting the in situ stress value



Acknowledgements The authors would like to thank all the supporters.

Funding This work was supported by the National Natural Science Foundation of China (51979152), Educational Commission of Hubei Province of China (T2020005), Open Foundation of Hydraulic Rock Mechanics of Ministry of Education (RMHSE1603), and Open Foundation of Hubei Key Laboratory of Construction and Management in Hydropower Engineering (2016KSD11).

References

- Bao H, Zhai Y, Lan HX et al (2019) Distribution characteristics and controlling factors of vertical joint spacing in sand-mud interbedded strata. *J Struct Geol* 128:103886. <https://doi.org/10.1016/j.jsg.2019.103886>
- Barton AAN (2000) TBM tunneling in jointed and faulted rock. Balkema, Rotterdam, pp 61–64
- Blümling P, Bernier F, Lebon P et al (2007) The excavation damaged zone in clay formations time-dependent behaviour and influence on performance assessment. *Phys Chem Earth* 32(8):588–599. <https://doi.org/10.1016/j.pce.2006.04.034>
- Cai M (2007) Influence of stress path on tunnel excavation response – numerical tool selection and modeling strategy. *Tunn Undergr Space Technol* 23(6):618–628. <https://doi.org/10.1016/j.tust.2007.11.005>
- Chu WJ (2009) Stability and structure safety assessment of surrounding rock in deep buried tunnel. Postdoctoral research report of Hydro China Huadong Engineering Corporation
- Cook NGW, Hoek E, Pretorius JPG et al (1966) Rock mechanics applied to the study of rockbursts. *J South Afr Inst Min Metall* 66(10):436–528
- Cundall P, Carranza-Torres C, Hart R (2003) A new constitutive model based on the Hoek–Brown criterion. In: Brummer R (ed) Proceedings of the 3rd international FLAC symposium. Balkema, Sudbury, pp 17–25
- Diederichs MS (2007) The 2003 Canadian geotechnical colloquium: mechanistic interpretation and practical application of damage and spalling prediction criteria for deep tunneling. *Can Geotech J* 44(9):1082–1116. <https://doi.org/10.1139/T07-033>
- Falls SD, Young RP (1998) Acoustic emission and ultrasonic-velocity methods used to characterize the excavation disturbance associated with deep tunnels in hard rock. *Tectonophysics*. 289(1–3):1–15. [https://doi.org/10.1016/S0040-1951\(97\)00303-X](https://doi.org/10.1016/S0040-1951(97)00303-X)
- Fan Y, Lu WB, Yan P et al (2015) Transient characters of energy changes induced by blasting excavation of deep-buried tunnels. *Tunn Undergr Space Technol* 49:9–17. <https://doi.org/10.1016/j.tust.2015.04.003>
- Fan Y, Lu WB, Zhou YH et al (2016) Influence of tunneling methods on the strainburst characteristics during the excavation of deep rock masses. *Engineering Geology* 201:85–95. <https://doi.org/10.1016/j.enggeo.2015.12.015>
- Field JE, Walley SM, Proud WG et al (2004) Review of experimental techniques for high rate deformation and shock studies. *Int J Impact Eng* 30(7):725–775. <https://doi.org/10.1016/j.ijimpeng.2004.03.005>
- Griffith AA (1921) The phenomena of rupture and flow in solids. *Philos Trans R Soc Lond A221*:163–198
- Hao XJ, Feng XT, Yang CX et al (2016) Analysis of EDZ development of columnar jointed rock mass in the Baihetan diversion tunnel. *Rock Mech Rock Eng* 49:1289–1312. <https://doi.org/10.1007/s00603-015-0829-4>
- Kwon S, Lee CS, Cho SJ et al (2009) An investigation of the excavation damaged zone at the KAERI underground research tunnel. *Tunn Undergr Space Technol* 24(1):1–13. <https://doi.org/10.1016/j.tust.2008.01.004>
- Li XB, Cao WZ, Zhou ZL et al (2014) Influence of stress path on excavation unloading response. *Tunn Undergr Space Technol* 42:237–246. <https://doi.org/10.1016/j.tust.2014.03.002>
- Liu Q, Xu X, Wu Z (2020) A GPU-based numerical manifold method for modeling the formation of the excavation damaged zone in deep rock tunnels. *Comput Geotech* 118:103351. <https://doi.org/10.1016/j.compgeo.2019.103351>
- Lu WB, Yang JH, Yan P et al (2012) Dynamic response of rock mass induced by the transient release of in-situ stress. *Int J Rock Mech Min Sci* 53:129–141. <https://doi.org/10.1016/j.ijmms.2012.05.001>
- Martin CD (1997) Seventeenth Canadian geotechnical colloquium: the effect of cohesion loss and stress path on brittle rock strength. *Can Geotech J* 34(5):698–725
- Martin CD, Read RS, Martino JB (1997) Observations of brittle failure around a circular test tunnel. *Int J Rock Mech Min Sci* 34(7):1065–1073. [https://doi.org/10.1016/s0148-9062\(97\)00296-9](https://doi.org/10.1016/s0148-9062(97)00296-9)
- Martino JB, Chandler NA (2004) Excavation-induced damage studies at the underground research laboratory. *Int J Rock Mech Min Sci* 41(8):1413–1426. <https://doi.org/10.1016/j.ijmms.2004.09.010>
- Mortazavi A, Molladavoodi H (2012) A numerical investigation of brittle rock damage model in deep underground openings. *Eng Fract Mech* 90:101–120. <https://doi.org/10.1016/j.engfractmech.2012.04.024>
- Pellet F, Roosefid M, Deleruyelle F (2009) On the 3D numerical modelling of the time-dependent development of the damage zone around underground galleries during and after excavation. *Tunn Undergr*

- Space Technol 24(6):665–674. <https://doi.org/10.1016/j.tust.2009.07.002>
- Read RS (2004) 20 years of excavation response studies at AECL's Underground Research Laboratory. *Int J Rock Mech Min Sci* 41(8):1251–1275. <https://doi.org/10.1016/j.ijmms.2004.09.012>
- Read RS, Martin CD, Dzik EJ (1995) Asymmetric borehole breakouts at the URL. The 35th US Symposium on Rock Mechanics (USRMS), Rotterdam, Balkema, 879–884.
- Siren T, Kantia P, Rinne M (2015) Considerations and observations of stress-induced and construction-induced excavation damage zone in crystalline rock. *Int J Rock Mech Min Sci* 73:165–174. <https://doi.org/10.1016/j.ijmms.2014.11.001>
- Souley M, Renaud V, Al Heib M et al (2018) Numerical investigation of the development of the excavation damaged zone around a deep polymetallic ore mine. *Int J Rock Mech Min Sci* 106:165–175. <https://doi.org/10.1016/j.ijmms.2018.04.028>
- Sun QH, Ma FS, Guo J et al (2020) Excavation-induced deformation and damage evolution of deep tunnels based on a realistic stress path. *Comput Geotech*:129. <https://doi.org/10.1016/j.compgeo.2020.103843>
- Tao M, Li XB, Li DY (2013) Rock failure induced by dynamic unloading under 3D stress state. *Theor Appl Fract Mech* 65:47–54. <https://doi.org/10.1016/j.tafmec.2013.05.007>
- Vazaios I, Vlachopoulos N, Diederichs MS (2019) Assessing fracturing mechanisms and evolution of excavation damaged zone of tunnels in interlocked rock masses at high stresses using a finite-discrete element approach. *J Rock Mech Geotech Eng* 11(4):701–722. <https://doi.org/10.1016/j.jrmge.2019.02.004>
- Wang SF, Li XB, Yao JR et al (2019) Experimental investigation of rock breakage by a conical pick and its application to non-explosive mechanized mining in deep hard rock. *Int J Rock Mech Min Sci* 122:104063. <https://doi.org/10.1016/j.ijmms.2019.104063>
- Wawersik WR, Fairhurst C (1970) A study of brittle rock fracture in laboratory compression experiments. *Int J Rock Mech Min Sci Geomech Abstr* 7(5):561–575
- Wu SY, Zhou JF, Chen BR, et al. (2015) Effect of excavation schemes of TBM on risk of rock burst of long tunnels at Jinping II hydropower station. *Chinese Journal of Rock Mechanics and Engineering*. 34(4): 728–734. DOI: 10.13722/j.cnki.jrme.2015.04.009 (in Chinese, Abstract in English)
- Xu ZL (2006) *Theory of elasticity*. China Higher Education Press, Beijing, pp 59–61 (in Chinese)
- Xu JB, Li H, Du K et al (2018) Field investigation of force and displacement within a strata slope using a real-time remote monitoring system. *Environ Earth Sci* 77(15):552–562. <https://doi.org/10.1007/s12665-018-7729-3>
- Yang JH, Yao C, Jiang QH et al (2017) 2D numerical analysis of rock damage induced by dynamic in-situ stress redistribution and blast loading in underground blasting excavation. *Tunn Undergr Space Technol* 70:221–232. <https://doi.org/10.1016/j.tust.2017.08.007>
- Yang JH, Jiang QH, Zhang QB et al (2018) Dynamic stress adjustment and rock damage during blasting excavation in a deep-buried circular tunnel. *Tunn Undergr Space Technol* 71:591–604. <https://doi.org/10.1016/j.tust.2017.10.010>
- Yong S, Kaiser PK, Loew S (2013) Rock mass response ahead of an advancing face in faulted shale. *Int J Rock Mech Min Sci* 60:301–311. <https://doi.org/10.1016/j.ijmms.2013.01.002>
- Young RP, Hazzard JF, Pettitt WS (2000) Seismic and micromechanical studies of rock fracture. *Geophysical Research Letters*. 27(12): 1767–1770. <https://doi.org/10.1029/2000GL011547>
- Zhang CS, Chen XR, Hou J et al (2010) Study of mechanical behavior of deep-buried marble at Jinping II hydropower station. *Chin J Rock Mech Eng* 29(10):1999–2009 (in Chinese, Abstract in English)
- Zhang QH, Li YJ, Yu MW et al (2015) Study of the rock foundation stability of the Aizhai suspension bridge over a deep canyon area in China. *Eng Geol* 198:65–77. <https://doi.org/10.1016/j.enggeo.2015.09.012>
- Zhu WC, Wei J, Zhao J et al (2014) 2D numerical simulation on excavation damaged zone induced by dynamic stress redistribution. *Tunn Undergr Space Technol* 43:315–326. <https://doi.org/10.1016/j.tust.2014.05.023>